Fragility estimate of railway bridges due to concrete fatigue

Fragility estimate of railway bridges due to concrete fatigue

Angelo Aloisio[a], Marco Martino Rosso[b,*], Massimo Fragiacomo[a], Rocco Alaggio[a]

[a] *Civil Environmental and Architectural Engineering Department, Università degli Studi dell'Aquila, via Giovanni Gronchi n.18, L'Aquila, 67100, Italy*
[b] *Politecnico di Torino, DISEG, Department of Structural, Geotechnical and Building Engineering, Corso Duca Degli Abruzzi, 24, Turin, 10128, Italy*

Abstract

Railway concrete bridges are prone to fatigue collapse, being subjected to multiple cyclic loads during their lifetime. This paper proposes a probabilistic procedure for assessing the fatigue life of concrete railway bridges. The procedure includes the uncertainties related to the concrete fatigue model and the concrete strength by highlighting the relevant uncertainty of existing fatigue models. Therefore, it proposes an enhancement of the fatigue model proposed by the Fib Code 2010 to reduce the modelling error possibly. The model has been calibrated on an extensive data set of normal-strength concrete samples following a Bayesian approach. Parallelly, the parameters have been reduced using a Bayesian step-wise deletion process. The paper uses the proposed probabilistic model to estimate the fragility curves in general cases by considering appropriate ranges for the train velocity, stress ratios and the number of cycles per year. In the second step, the paper applies the procedure to the fragility estimate of a typical prestressed-concrete railway bridge. The bridge response has been estimated using a finite-difference (FD) model. The FD model, simulating train-track-bridge interaction, has been calibrated on the measured displacement response. The analyses have been referred to different scenarios when suitable ranges of train velocities and cycles per year are considered.

Keywords: Concrete fatigue model, Fragility curves, Railway bridges, Probabilistic models, Bayesian calibration, Train-track-bridge interaction, Bridge dynamics, Finite difference approximation, Train loads

*Corresponding author.
Email address: marco.rosso@polito.it (Marco Martino Rosso)

1. Introduction

Fatigue represents a potential failure mechanism for structures under repetitive loadings, such as traffic loads [12]. Steel structures are particularly prone to fatigue. However, also concrete structures can suffer from fatigue cracking [46]. Nonetheless, compared to steel, fatigue phenomena in concrete are less predictable. Current design codes, such as the Eurocodes (EN1992-1-1, EN1992-2, EN1991-2), include extended rules for fatigue analysis and design of concrete bridges.

Fatigue significantly affects the life cycle of concrete. Multiple experimental investigations proved that the fatigue life of concrete decreases dramatically with an increase in the maximum tensile stress level [48]. Currently, there are two main approaches for predicting the fatigue life of concrete structures, a mechanics-based and an empirical method. Both methods suffer from several flaws, which compromise the successful application of these methods to concrete structures. The mechanics-based approach is based on fracture mechanics. It aims to analyze crack initiation and propagation. The most widely used fatigue crack growth model was proposed by Paris, which relates the crack growth rate and stress-intensity factor range [44]. In steel structures, Miner's rule is applied for fatigue evaluation considering the linear damage accumulation [22]. In concrete structures, ASHTO, AREMA, BBK 04, BS 5400, Eurocode 2, fib Model Code 2010, and SIA D 1033 specifications recommend that fatigue damage in concrete structures should be estimated using the Palmgren–Miner rule [40].

However, the prediction of crack propagation in concrete is a complex phenomenon, influenced by multiple factors, including concrete strength, reinforcing steel strength, and bonding behaviour [60]. Experimental fatigue tests on concrete samples highlight a wide scatter of cycles to failure under the same conditions. The discrepancy between cycles to failure of concrete specimens with identical load conditions under fatigue can be huge, spanning from 100 to 100000 cycles [49]. The high scattering of experimental data compromises the successful application of mechanics-based models. Besides, the scholar does not possess adequate knowledge of structural defects, which can trigger crack propagation. Therefore, mechanics-based approaches cannot be considered feasible methods in engineering practice.

Fatigue phenomena in concrete generally demand an empirical approach. The complexity for treating and interpreting experimental results and the significant time-cost of fatigue tests fed elementary approaches based on S-N

curves [31] see Eurocode 2 [53] and Model Code 2010 [59]. These design methods indicate the expected number of cycles to failure for specific maximum stresses. However, the S-N curve approach has several flaws.

- S-N curves are successfully applied to steel structures. However, the huge dispersion of fatigue results for concrete does not allow a straightforward deterministic approach. There are several S-N curves for concrete calibrated on experimental data. Still, fatigue models from literature or code are highly conservative. They are useful for identifying the conditions where fatigue failure is unlikely to occur. Nonetheless, these models cannot be considered predictive due to the large modelling error.

- S-N curves are calibrated on experimental samples loaded under a specific stress level (S). However, traffic loads on bridge structures lead to a wide range of stress levels during service life. Therefore, S-N curves cannot directly predict bridge fatigue life.

- The macroscopic or phenomenological approach does not directly consider the physical mechanism of fatigue damage [33].

Under bending fatigue loads, the stress distribution in the cross-section is not uniform. Hence, fatigue damage's progress differs at different cross-section depths [27]. This phenomenon leads to a stress-redistribution over the cross-section, which causes a variable stress ratio during the fatigue life. As a result, the stress levels of concrete and steel change over fatigue cycles. These phenomena, observed by several scholars [7, 26], are essential and must be considered when assessing the fatigue life of concrete structures. Nonetheless, the difficulty in tracking the time evolution of the stress ratio further supports a macroscopic approach. S-N curves for eccentric compression are calculated with the initial stress ratio, although it varies as the cycles accumulate and affects the failure. Therefore, the authors will follow an empirical approach where the stress ratio is assumed to be constant and equal to the initial one. At the same time, a probabilistic model for the S-N curves will be used to predict the cycles to failure. The S-N curves are obtained from experimental tests and possess information about stress redistribution caused by eccentric loading.

There is no well-acknowledged procedure for estimating the fatigue life of concrete structures. Many researchers agree on the need for a probabilistic approach to fatigue. In some studies, fatigue uncertainty is related

to the randomness of the material properties [36, 58, 37]. Multiple probability density functions have been considered, such as the log-normal or Birnbaum-Saunders [38, 42, 47]. Recent papers highlight that fatigue results follow a Weibull distribution, with two or three parameters [49, 1, 9]. Castillo and Fernández-Canteli [10] proved that Weibull and Gumbel are the only distributions applicable to fatigue based on the weakest-link hypothesis, compatibility conditions and asymptotic properties. Different fatigue models have been developed based on one of these distributions by giving a physical meaning to the distribution parameters or relating them to some other empirical parameters fitted through experimental tests [49]. The concrete fatigue behaviour is highly different in tension and compression. This investigation focuses on fatigue performance under compression since fully prestressed concrete girders are selected as reference structures. Accordingly, the probabilistic fatigue model is based on compressive fatigue tests.

To the authors' knowledge, there is no research on the effect of fatigue model uncertainty on the fatigue life prediction of concrete railway bridges under repetitive loading. This paper introduces the concept of fatigue life and proposes a probability-based method for estimating the fragility curves due to fatigue. The reliability analysis includes all uncertainties related to concrete strength, fatigue model, expected load conditions, and predictive model of the bridge response. After a theoretical introduction, the procedure supports a discussion based on extensive parametric analyses. Then, the proposed method is applied to an ordinary railway concrete bridge. Estimating the fragility curves has required the development of predictive models of fatigue and bridge response.

Fatigue models of technical provisions are deterministic and not suitable for reliability analyses. Furthermore, probabilistic fatigue models from the literature are characterized by a significant modelling error, undermining the usefulness of reliability analyses. Consequently, there is a need for a more accurate probabilistic model of concrete fatigue, allowing its use within current technical standards. Following the general procedure in [21], the present paper proposes a probabilistic model derived from the Fib Model Code 2010 to predict the number of fatigue cycles to failure. The model is formulated by adding suitable correction terms to the predictive equation from the Fib Model Code formulation. The correction terms include explanatory functions calibrated and selected through a Bayesian approach using the experimental data collected by [57]. The accuracy of the proposed models is compared with that of a linear model and the one proposed by the Fib Code 2010. The

stress level is estimated from a finite difference model of the bridge response, which models the Train-Track-Bridge Interaction (TTBI).

It must be remarked that the fatigue performance of concrete and steel reinforcements determines the fatigue life of a concrete bridge. In some tests on RC beams subjected to fatigue loads, failure stems from fatigue fracture of steel reinforcements. An RC beam should be considered a serial system since failure might occur if either concrete or steel reaches the fatigue cracking. However, this paper will focus on the sole concrete contribution to fatigue to prove the significant uncertainty related to its estimation. Isolating the concrete contribution to fatigue will allow assigning the related uncertainty in the fatigue life estimate to the sole concrete.

Several papers on TTBI, like [19], with experimental validation, prove that elementary approaches based on beam models for the track and the bridge with viscoelastic coupling can accurately seize the experimental displacement response with a minor error, compared to more advanced models of the TTBI [4]. The growth of the model complexity leads to increased model parameters being calibrated. The growth in complexity can add significant uncertainty to the mathematical model and dramatically increase the computational effort. Besides, sophisticated models can only be created with great effort and do not allow parametric studies or stochastic simulations due to the high computational cost. To develop and validate a general procedure for estimating the fatigue life of concrete railway bridges, the paper presents an elementary finite difference model of the TTBI, which can be easily used for parametric analyses and Monte Carlo simulations. The governing equations of the track and the bridge, modelled as Euler-Bernoulli beams, are coupled by a distributed layer of springs representing the ballast. The two equations are solved under a moving load excitation using a Runge–Kutta family and the finite-difference method for the temporal and spatial discretization, respectively. The authors validated the mathematical model of the TBBI against the displacement response of rail bridges with a ballasted sub-structure.

In conclusion, the novel contributions of this article can be summarized as follows:

- Probabilistic improvement of the fatigue model in the Fib Code 2010 for estimating the fatigue life of concrete railway bridges. The probabilistic correction is obtained by adding suitable explanatory functions to the deterministic predictive equation. The model aims to reduce the

modelling error for the reliability analysis.

- Development of a finite difference model to evaluate the structural response of a non-classically damped Euler-Bernoulli beam under a moving load excitation. The model has been validated with the experimental displacement response of a ballasted bridge under train loads. The model parameters have been optimized using a genetic optimization algorithm.
- Assessing the effects of stress levels, fatigue model uncertainty, traffic intensity, and train velocity on the fatigue life of concrete railway structures.
- Application of the proposed method to a short-span ordinary concrete bridge.

The paper has the following organization. After the introduction section, the paper presents the probabilistic framework for estimating the fragility curves and the fatigue life. The third section describes the TTBI model used to estimate stress levels, while the fourth section presents and discusses the proposed probabilistic fatigue model. The fifth section presents parametric analyses, where multiple fragility curves are estimated by varying the stress levels, the train velocity, the expected train traffic, and the fatigue model's standard deviation. In the sixth section, the proposed procedure for the fragility curve assessment is applied to a full-scale railway bridge. This section discusses the practical implications of estimating the fatigue life following the proposed method.

2. Fragility curves and fatigue life estimation

The output of fatigue tests is the number of cycles to failure. Fatigue tests do not provide the strength reduction of concrete samples due to cyclic loads. Therefore, the limit state function for fatigue failure mechanisms cannot be written in terms of static or kinematic variables. Fatigue failure may occur if the load cycles exceed the predicted number of cycles to failure. Accordingly, the limit state function can be written as the difference between the predicted number of cycles to failure, representing the capacity, and the expected number of load cycles, expressing the demand.

The limit state function can be formulated as

$$g\left(\mathbf{r}, \mathbf{p}, \hat{\mathbf{s}}, n_y, \boldsymbol{\Theta}\right) = C\left(\mathbf{r}, \hat{\mathbf{s}}, \boldsymbol{\Theta}\right) - D\left(\mathbf{r}, \mathbf{p}, \hat{\mathbf{s}}, n_y, \boldsymbol{\Theta}\right) \tag{1}$$

where $C\left(\mathbf{r}, \hat{\mathbf{s}}, \boldsymbol{\Theta}\right)$ is the number of cycles to failure obtained from the probabilistic fatigue model, $D\left(\mathbf{r}, \mathbf{p}, \hat{\mathbf{s}}, n_y, \boldsymbol{\Theta}\right)$ is the cumulated expected number of cycles at a given year obtained from the probabilistic demand model. In detail, $\mathbf{r}$ collects the material properties of the bridge (e.g., concrete resistance), $\mathbf{p}$ collects all information regarding the load excitation (train length, train weight, train velocity, number of trains per years, e.g.), $\hat{\mathbf{s}}$ indicates the reference stress ratio used to homogenize the number of load cycles of the capacity and demand models, n_y is the number of years. The stress ratio is the ratio between the maximum or minimum stress and the material resistance.

Theoretically, It would be possible to calibrate two probabilistic models, one for the capacity and one for the demand. The probabilistic capacity model has been calibrated on experimental compressive fatigue tests. Conversely, the demand model is assumed deterministic since the authors do not possess experimental data associated with multiple train transits from permanent structural monitoring. Therefore, the lack of an adequate number of experimental data for the bridge response does not allow the calibration of a probabilistic demand model.

The limit state function can be used to compute the fragility of a given structure. Fragility functions define the conditional probability of meeting or exceeding a prescribed limit state for a given value of the demand measure. If the demand is expressed in terms of the number of cyclic loads per year, the increasing number of years can be considered as a suitable intensity measure for fragility estimation. The events associated with a limit state function less or equal to zero define the failure related to the considered phenomenon. Rigorously, following Equation (1) the fragility of a given structure can be written as

$$F\left(\mathbf{r}, \mathbf{p}, \hat{\mathbf{s}}, n_y, \boldsymbol{\Theta}\right) = P\left[\{g(\mathbf{r}, \mathbf{p}, \hat{\mathbf{s}}, n_y, \boldsymbol{\Theta}) \leq 0\} \,|n_y\right] \tag{2}$$

Empirical fragilities are estimated using direct Monte Carlo simulations [2]. The failure probability is obtained by dividing the number of simulations associated with exceeding the number of cycles to failure and the total number of simulations.The expected fatigue life in years ($\hat{n}_y$) can be obtained from the fragility curves:

$$\text{Find } \hat{n}_y \;:\; \beta(\mathbf{r}, \mathbf{p}, \hat{\mathbf{s}}, n_y) = \hat{\beta} \tag{3}$$

where $\hat{\beta}$ is the reference reliability threshold provided by the code. Table 1

Table 1: Target β-values for elements (lifetime), ISO 2394:1998 [54].

Relative costs of	Consequences of failure			
safety measures	small	some	moderate	great
Low	0	1.5	2.3	3.1
Moderate	1.3	2.3	3.1	3.8
High	**2.3**	3.1	3.8	4.3

provides target β-values for structural elements (lifetime) according to ISO 2394:1998 [54].

Compared to steel, fatigue in concrete has minor consequences of failure: the steel reinforcement prevents the dramatic consequences of brittle failure due to the crack opening. Therefore, fatigue failure in concrete structures has no direct consequences on global collapse. The cracks can trigger corrosion phenomena and further cracking due to the increment in the stress level. However, fatigue cracks in concrete structures with shear and bending reinforcement have no direct consequences on global collapse. Parallelly, the costs of safety measures would be high. As discussed in the following sections, it is possible to prevent fatigue cracks by reducing the stress values inside the structure. This can only be achieved by replacing the structure or adopting invasive structural interventions. Therefore, the reliability target corresponding to high relative costs for safety measures and minor consequences of failure is 2.3; see Table 1.

This paper uses $\hat{\beta} = 2.3$ to estimate the fatigue life of railway-reinforced concrete bridges. The fatigue life cannot be considered the expected duration of a structure before it collapses. The occurrence of fatigue cracking does not lead to failure in structures with adequate steel reinforcement. Therefore, the fatigue life can be considered a time limit beyond which it is appropriate to verify the integrity of concrete through extensive tests and, in the case of cracks, adopt adequate safety measures to limit the consequences of the fatigue cracks (corrosion, e.g.).

2.1. Capacity model

The limit state function compares the expected number of cycles to failure and the expected number of cyclic loads. Following [21], the number of cycles

to failure, i.e. the capacity, can be written as:

$$T\left[C\left(\mathbf{r},\hat{\mathbf{s}},\boldsymbol{\Theta}\right)\right]=T\left[\hat{C}\left(\mathbf{r},\hat{\mathbf{s}}\right)\right]+\gamma\left(\mathbf{r},\hat{\mathbf{s}},\boldsymbol{\theta}\right)+\sigma\varepsilon, \tag{4}$$

where $T(\cdot)$ is a variance stabilizing transformation, $C(\mathbf{r},\hat{\mathbf{s}},\boldsymbol{\Theta})$ is the total number of cycles to failure, while $\boldsymbol{\Theta}=\{\boldsymbol{\theta},\sigma\}$ are unknown model parameters. On the right side of Equation ((4)), $\hat{C}\left(\mathbf{r},\hat{\mathbf{s}}\right)$ is the capacity according to a deterministic fatigue model; generally a physics-based model dependent on the specific engineering problem [13, 3, 2, 5, 39], $\gamma\left(\mathbf{r},\hat{\mathbf{s}},\boldsymbol{\theta}\right)$ is a correction term based on pieces of evidence from the experimental data. The product $\sigma\varepsilon$ is the model error, with model standard deviation σ and normally distributed random variable ε. The model is based on three assumptions: additivity (i.e., the additivity of $\sigma\varepsilon$); homoskedasticity (i.e., the independence of σ from $\mathbf{r}$ and $\hat{\mathbf{s}}$); normality (i.e., the normality of ε). Through a suitable choice of $T(\cdot)$, such assumptions can be approximately satisfied in the transformed space within the range of the data used to calibrate the model. Following the traditional approach of the fatigue model, the logarithm to base ten is chosen as variance stabilizing transformation.

2.2. Demand model

The demand model gives the expected number of cycles cumulated at a given year n_y. By assuming a probabilistic model of the number of load cycles per year, the demand model can be written as follows:

$$D\left(\mathbf{r},\mathbf{p},\hat{\mathbf{s}},n_y,\boldsymbol{\Theta}\right)=n_y\left[D_y\left(\mathbf{r},\mathbf{p},\hat{\mathbf{s}},\boldsymbol{\Theta}\right)\right] \tag{5}$$

The expected number of load cycles per year ($D_y\left(\mathbf{r},\mathbf{p},\hat{\mathbf{s}},\boldsymbol{\Theta}\right)$) cannot be directly obtained from the database collecting the details of the train traffic of the past years. The traffic load includes many train loads, typologies and velocities. Therefore, the load cycles caused by the traffic load vary in amplitude and stress level. However, according to existing fatigue models, the number of cycles to failure always refers to a given stress level, generally expressed as the ratio between the maximum stress and material resistance.

As highlighted in the description of Equation (1), the number of cycles for capacity and demand are homogenized to a given stress level, defined by vector $\hat{\mathbf{s}}$, collecting the maximum and minimum stress ratios.
The expected number of homogenized cycles per year can be estimated as follows:

$$D_y\left(\mathbf{r},\mathbf{p},\hat{\mathbf{s}},\boldsymbol{\Theta}\right)=\sum_{i=1}^{n_t}\frac{l_i}{2n_{v,i}}\cdot\mathcal{H}\left(\mathbf{r},\mathbf{s}_i,\hat{\mathbf{s}},\boldsymbol{\Theta}\right) \tag{6}$$

where i indicates the i-th train, n_t the total number of trains per year, l_i the length of the i-th train, $n_{v,i}$ the number of vehicles of the i-th train, while $\mathcal{H}_i(\mathbf{r}, \hat{\mathbf{s}}, \mathbf{s}_i, \boldsymbol{\Theta})$ is an homogenization factor.
The homogenization factor can be expressed in terms of the capacity model. The number of load cycles can be homogenized to their effect on fatigue, given the stress level associated with the cycle. The $\mathcal{H}_i(\mathbf{r}, \mathbf{s}_i, \hat{\mathbf{s}}, \boldsymbol{\Theta})$ factor can be written as:

$$\mathcal{H}_i(\mathbf{r}, \mathbf{s_i}, \hat{\mathbf{s}}, \boldsymbol{\Theta}) = \frac{C(\mathbf{r}, \mathbf{s}_i, \boldsymbol{\Theta})}{C(\mathbf{r}, \hat{\mathbf{s}}, \boldsymbol{\Theta})} \tag{7}$$

where $\mathbf{s}_i$ is the stress ratio associated with the i-th train, while $\hat{\mathbf{s}}_i$ is the reference stress ratio. The proposed homogenization approach does not explicitly consider the load sequence's effect since it adopts a linear scaling based on the stress level. This approach follows current design codes, which estimate the fatigue life under variable amplitudes using the Palmgren–Miner (P-M) [43] rule and assumes a linear scaling between lifetimes measured for uniform cyclic loading scenarios. Nonetheless, the load sequence effect observed in compression by Holmen [23] and Petkovic et al. [45] showed that the well-known P–M rule might lead to inaccurate fatigue life estimations, as recently confirmed by [6]. Therefore, future research efforts will include the load sequence effect for predicting the fatigue life of concrete structures under generally variable fatigue loading scenarios.

2.3. Discussion

The proposed probabilistic framework for estimating the fatigue life of concrete railway bridges might merit the discussion of the following aspects:

- Considered sources of uncertainty;
- Homogenization approach;
- Number of cyclic loads estimation.

The paper only considers the uncertainty of the fatigue model and material resistance, which affect the capacity and the demand through the homogenization factor. The scholar could also treat the expected train traffic per year as a vector of random variables. It could be possible to estimate the variation of the railway traffic between years by modifying Equation (5). The demand at a given year could be obtained by multiplying the expected demand per year by a time-dependent factor that amplifies or reduces the

trainload during the lifetime. However, train traffic does not exhibit a significant variation across the years. This fact will be confirmed in the following sections by showing the traffic variation of a sample bridge in the period 2017-2021.

The managing bodies of the Italian railway network distinguish three traffic categories:

- $n_{t,d}$ <40-Low traffic
- $40 \leq n_{t,d} \leq 100$-Moderate traffic
- $n_{t,d} > 100$-High traffic

where $n_{t,d}$ is the expected number of trains per day. The results shown in the following sections prove that the effect of the traffic load per day can be negligible if the fatigue model has significant uncertainty. Therefore, modelling the train traffic as a vector of random variables could be considered unnecessary for this research. The paper will show that the fatigue model is the weak link of the entire framework. Therefore, refining the load estimate has no significant effect on improving the accuracy of the prediction.

The entire framework is based on a homogenization approach. This aspect represents an element of originality. It derives from the existing fatigue model's limitation, which does not predict the number of cycles to failure if the stress level changes during the loading phase. Experimental fatigue tests impose a constant stress level during the cycles. Experimental fatigue tests with a variable load protocol would add additional scatter to the results, which are already difficult to interpret. Therefore, the capacity model can only give the number of cycles to failure for a given stress level. Parallelly, the train traffic causes load cycles variable in amplitude. Therefore, if a reference stress level is assumed for the capacity estimation, expressed by the vector $\hat{\boldsymbol{s}}$, each load cycle caused by the train must be set equivalent to the reference stress level. Specifically, each load cycle causes specific stress values in the bridge cross-section. The fatigue model can be used to set an equivalence between the number of load cycles and stress levels based on the number of cycles to failure corresponding to the stress due to the i-th train transit ($\boldsymbol{s_i}$) and the reference one ($\hat{\boldsymbol{s}}$), assumed in the analyses.

The computing of the number of load cycles is based on the geometric details of the train; see Equation (6). Figure 1 shows a schematization of the train model. Experimental investigations, see [19], proved that a load cycle is

generally associated with the transit of two train axes corresponding to two vehicles. As shown in the next section, this evidence supports modelling two train axes with an equivalent concentrated force. The succession of almost

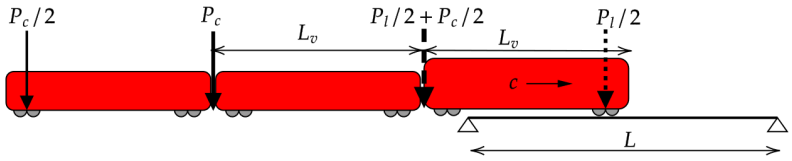

Figure 1: Schematization of the train loads.

equally spaced concentrated forces generates a cyclic excitation to the bridge with frequency f_{dominant}, [28]:

$$f_{\text{dominant}} = \frac{n_{v,i}}{l_i} \tag{8}$$

where $n_{v,i}$ and l_i are defined after Equation (6). As remarked by several scholars [20], the dynamic amplification factor in railway bridges is close to unit and generally below 2. The dynamic amplification depends on the adimensional velocity of the train, defined as:

$$\alpha = \frac{f_{\text{dominant}}}{f_1} \tag{9}$$

where f_{dominant} is defined in Equation (8), and f_1 is the first natural frequency of the bridge. Interestingly, in low and medium-span bridges, the dynamic effect of the loads does not cause an increment in the number of load cycles due to the interaction between the excitation frequency (f_{dominant}) and the modal parameters of the bridge. After the last train vehicle left the bridge, the bridge did not significantly manifest oscillation, as confirmed by the experimental tests used to validate the proposed bridge model. Therefore, the number of load cycles can be estimated from the train characteristics, while the stress level ($\boldsymbol{s}$), caused by the train, is from the mechanical model of the bridge.

3. Bridge modeling

The stress level vector of the i-th train collects the maximum and minimum stress ratios reached during the load cycles:

$$\mathbf{s}_i = \{S_{c,\text{max}.i}, S_{c,\text{min},i}\} \tag{10}$$

$$S_{c,\max,i} = \frac{\sigma_{c,\max}, i}{f_c} \tag{11}$$

$$S_{c,\min,i} = \frac{\sigma_{c,\min}, i}{f_c} \tag{12}$$

where f_c is the concrete resistance, $\sigma_{c,\max}$, and $\sigma_{c,\min}$ are the maximum and minimum stresses during the load cycles corresponding to the i-th train transit. The concrete resistance is considered a random variable:

$$f_c = f_{cm} + \sigma_c \varepsilon \tag{13}$$

where f_{cm} is the mean concrete strength referred to as the concrete resistance class of the bridge. At the same time, the product $\sigma_c \varepsilon$ expresses the resistance scatter, with standard deviation σ_c and normally distributed random variable ε. For the sake of simplicity, a constant value for σ_c is adopted. Specifically, based on the extensive investigation by Shimizu et al. [51], the adopted coefficient of variation for f_{cm} is equal to 0.20.

The maximum and minimum stresses should be obtained from a TTBI model as follows:

$$\boldsymbol{\sigma}_{c,\max,i} = \mathcal{M}(\boldsymbol{p}_i) \tag{14}$$

where $\mathcal{M}$ is the TTBI model, and $\boldsymbol{p}_i$, following the notation in Equation (1), collects the information of the i-th train. The bridge model ($\mathcal{M}$) is obtained from the separate modelling of the bridge and the track. Therefore, this section is divided into four subsections dedicated to the track and bridge modelling and to the temporal and spatial discretization of the governing equations. Appendix A details the TTBI model.

4. Probabilistic Fatigue model

This section proposes a novel probabilistic fatigue model of concrete derived from the Fib Model 2010 by adding suitable correction terms. Recent models for concrete fatigue are generally validated against high-strength concrete data [32, 52, 17, 18, 24, 29, 34, 35]. However, most of the reinforced concrete railway bridges are made of normal strength concrete. Therefore, following [32], the probabilistic fatigue model is developed using a database of 219 tests of normal-strength concrete samples. The test results are taken from the scientific literature [50, 56, 25, 30, 23].

The paper considers reference structures for estimating the fatigue life of a fully prestressed concrete girder. Therefore, these structures experience

cyclic eccentric compressive loads during their service life. Therefore, theoretically, the probabilistic fatigue model should be calibrated on eccentric compressive tests. However, the lack of experimental tests on eccentric compression forced the authors to collect a database including pure compression tests. Nonetheless, the major difference in the concrete fatigue behaviour depends on the stress sign between tension and compression rather than the occurrence of eccentric compression. No tension is supposed to occur in the structure due to the full prestress condition.

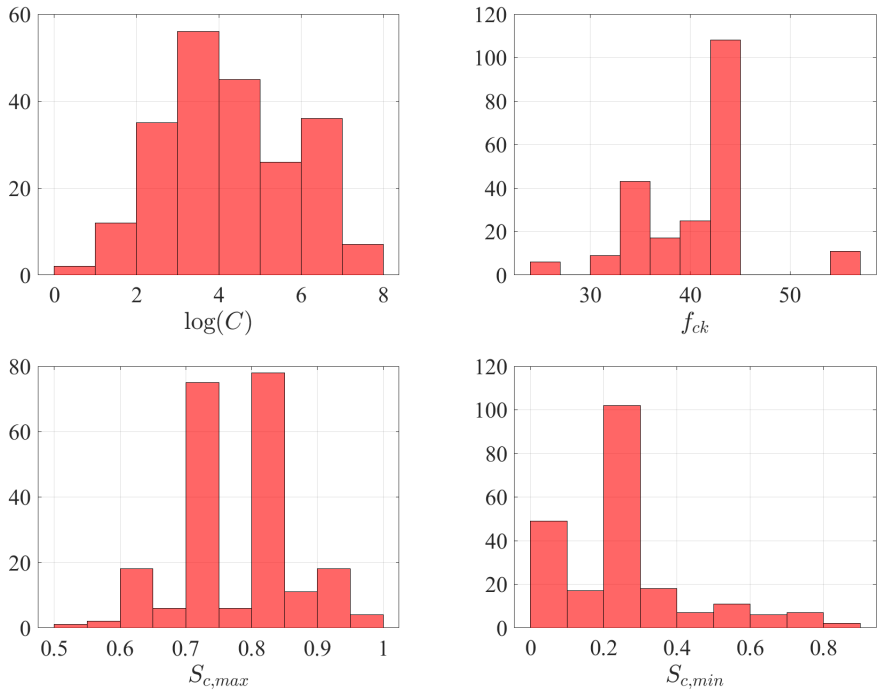

Figure 2: Histogram plot of the experimental data of fatigue tests used for the model calibration, following [32].

Figure 2 shows the histogram plots of the test data in terms of the number of cycles to failure (C), concrete strength (f_{ck}), and maximum ($S_{c,max}$) and minimum ($S_{c,min}$) stress levels. The number of cycles to failure reaches 10^7 in some concrete specimens, while most fail at nearly 10^4. The concrete strength is between 20 and 70 MPa, although the largest percentage of samples has a 44MPa compression strength. The maximum stress level is quite significant for all specimens. There are no data for $S_{c,max} < 0.5$. This fact

represents the main limitation of existing databases of fatigue tests. Most structures experience a maximum stress level lower than 0.5, not excessively exploiting the material potential. Therefore, the proposed fatigue model, like the literature ones, will be extrapolated to estimate the number of failure cycles when moderate stress levels occur. Moreover, testing concrete specimens with a stress level lower than 0.5 would require extremely time-consuming experimental tests.

4.1. Model formulation and calibration

The model for concrete fatigue follows the structure in Equation (4):

$$\log\left[C\left(\mathbf{r},\hat{\mathbf{s}},\boldsymbol{\Theta}\right)\right]=\log\left[\hat{C}\left(\mathbf{r},\hat{\mathbf{s}}\right)\right]+\gamma\left(\mathbf{r},\hat{\mathbf{s}},\boldsymbol{\theta}\right)+\sigma\varepsilon, \tag{15}$$

The correction term $\gamma\left(\mathbf{r},\boldsymbol{\theta}\right)$ is selected as a linear combination of n dimensionless explanatory functions $h_i(\mathbf{r})$ and reads:

$$\gamma\left(\mathbf{r},\hat{\mathbf{s}},\boldsymbol{\theta}\right)=\boldsymbol{\theta}^{\mathrm{T}}\cdot\mathbf{h}\left(\mathbf{r},\hat{\mathbf{s}}\right). \tag{16}$$

The considered set of explanatory functions $\mathbf{h}\left(\mathbf{r}\right)=\left\{h_1\left(\mathbf{r}\right),..,h_n\left(\mathbf{r}\right)\right\}$ is obtained by combining the three variables affecting $\hat{C}\left(\mathbf{r}\right)$: $S_{c,\max}$, $S_{c,\min}$, collected in $\hat{\mathbf{s}}$, and f_{ck} in $\mathbf{r}$. $\mathbf{r}$ collects the material properties of the bridge (e.g., concrete resistance).

The number of variables involved in the capacity model is limited by those reported in the experimental fatigue tests. The variables are three: the maximum and minimum stress ratios and the concrete compressive strength. Hence, the authors, rather than checking by hand which combinations between the three parameters correspond to a significant regressor, adopted an automatic approach by taking all combinations between them and then a posteriori selecting the relevant ones with a step-wise procedure. The explanatory functions should be dimensionless to determine a general, size-independent model. However, using dimensionless explanatory functions is a recommendation to achieve a general model, although in some circumstances selecting dimension variables does not impair the rigour of the procedure. In this situation, next to the dimensionless stress ratios, the compressive strength was also included to observe possible phenomena related to its influence on the fatigue capacity. It is known that compressive strength can affect the fatigue performance of concrete.

The three variables are multiplied and raised to the i-th, j-th and z-th power, respectively. The explanatory functions are generated by taking

all possible combinations between i, j, and z, where $\{i, j, z\} \in \mathbb{N}$ and $0 \leq \{i, j, z\} \leq n_{\max}$ with $n_{\max}$ the maximum model order. All combinations $\{i, j, z\}$ are collected in a set S. The generic combination from the set S is a subset of three ($k = 3$) distinct elements of S. Therefore, the cardinality of S is equal to the binomial coefficient.

$$h\left(\mathbf{r}\right)_{ijz} = S^{i}_{c,\max} S^{j}_{c,\min} f^{z}_{ck} \mid \mathrm{card}(S) = \binom{3n_{\max}}{3} \tag{17}$$

Given a maximum model order ($n_{\max}$) equal to three, i.e. the maximum exponent between i, j and z, the number of regressors from Equation 16 is equal to 84.

The parameters collected into $\mathbf{\Theta}$ are calibrated using the Bayesian approach [8]. This method combines the prior knowledge on the parameters, which is contained in the prior distribution of $\mathbf{\Theta}$, $f'(\mathbf{\Theta})$, with the information provided by the data, which is contained in the likelihood function, $\mathcal{L}(\mathbf{\Theta})$. The posterior distribution of the parameters $f''(\mathbf{\Theta})$ is defined as follows:

$$f''\left(\mathbf{\Theta}\right) = k\mathcal{L}\left(\mathbf{\Theta}\right) f'\left(\mathbf{\Theta}\right), \tag{18}$$

and it is obtained by dividing the product $\mathcal{L}(\mathbf{\Theta})f'(\mathbf{\Theta})$ by the evidence k, which is the following normalizing constant:

$$k^{-1} = \left[\int_{\Omega_{\mathbf{\Theta}}} \mathcal{L}\left(\mathbf{\Theta}\right) f'\left(\mathbf{\Theta}\right) \mathrm{d}\mathbf{\Theta}\right], \tag{19}$$

where $\Omega_{\mathbf{\Theta}}$ is the parameters space. The posterior distributions $f''(\mathbf{\Theta})$ obtained after the calibration can be used to find a point estimate for the model by ignoring the epistemic uncertainties in the model parameters. An alternative approach is used in the present study, which also accounts for the epistemic uncertainties in the model parameters. This alternative approach assumes $\mathbf{\Theta}$ as random variables and find a predictive estimate of $C(\mathbf{r}, \hat{\mathbf{s}}, \mathbf{\Theta})$ in agreement with [21] as follows:

$$\tilde{C}\left(\mathbf{r}, \hat{\mathbf{s}}\right) = \int_{\Omega_{\mathbf{\Theta}}} C\left(\mathbf{r}, \hat{\mathbf{s}}; \mathbf{\Theta}\right) f''\left(\mathbf{\Theta}\right) \mathrm{d}\mathbf{\Theta}. \tag{20}$$

Since an analytical solution for Equation ((20)) is often missing, it is opportune to find a numerical approximation of the distribution of $\tilde{C}\left(\mathbf{r}, \hat{\mathbf{s}}\right)$ by sampling from $f''(\mathbf{\Theta})$ and finding the corresponding realizations of $C(\mathbf{r}, \hat{\mathbf{s}}; \mathbf{\Theta})$.

Non-informative priors are chosen in the form of Gaussian distribution with zero means and large variance for all the parameters. To facilitate the use of the model and its possible implementation into technical standards, it should be parsimonious (i.e., with a correction term constructed using a limited number of explanatory functions n) and as accurate as possible (i.e., with a small value of standard deviation σ). However, a reduction of n usually entails a higher value of σ. Therefore, the model has been reduced by following a step-wise deletion of the parameters. The step-wise deletion process allows finding a trade-off between parsimony and accuracy [55]. The stepwise deletion process used in this paper starts with a model that includes all the candidate explanatory functions and at each step, removes the explanatory function with the highest coefficient of variation (COV) of the corresponding θ_i, as proposed in [21]. Once an explanatory function is removed, the model is re-calibrated and the deletion process is repeated. The deletion process ends when either σ grows beyond an undesirable threshold or the increment of σ is too large compared to the reduction of the model complexity. Fig.3 shows a workflow of the procedure from the initial to the reduced model formulation

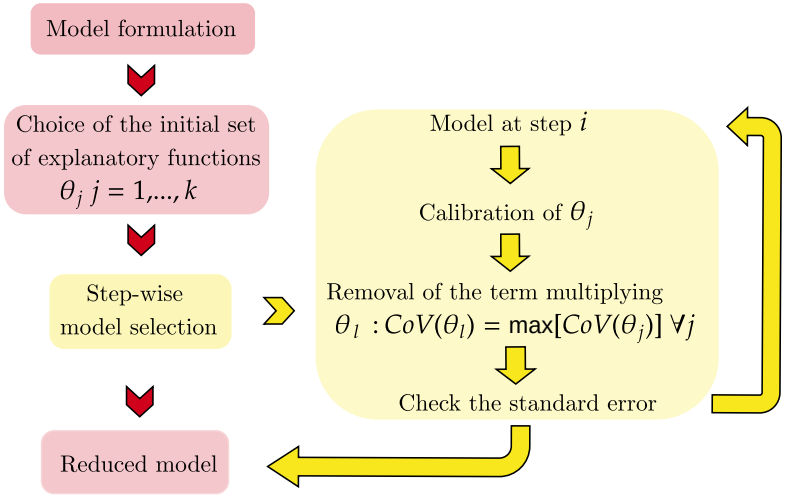

Figure 3: Workflow of the procedure from the initial to the reduced model formulation.

4.2. Deterministic fatigue model

The deterministic capacity equation is taken from the fib Model Code 2010 [12]:

$$\log\left[\hat{C}\left(\mathbf{r},\hat{\mathbf{s}}\right)\right] = \begin{cases} \log N_1, & \text{if } \log N_1 \leq 8 \\ \log N_2 & \text{if } \log N_1 > 8 \end{cases} \tag{21}$$

where N_1 and N_2 are the numbers of cycles to failure. The two S–N relations for N_1 and N_2 if $0 \leq S_{c,min} \leq 0.8$) read:

$$\log N_1 = \frac{8}{Y-1}\left(S_{c,\max} - 1\right) \tag{22}$$

$$\log N_2 = 8 + \frac{8\ln(10)}{Y-1}\left(Y - S_{c,\min}\right)\log\left(\frac{S_{c,\max} - S_{c,min}}{Y - S_{c,\min}}\right) \tag{23}$$

where,

$$Y = \frac{0.45 + 1.8S_{c,\min}}{1 + 0.85S_{c,\min} - 0.3S_{c,\min}^2} \tag{24}$$

$$S_{c,\max} = \frac{\sigma_{c,\max}}{f_{ck,\text{fat}}} \tag{25}$$

$$S_{c,\min} = \frac{\sigma_{c,\min}}{f_{ck,\text{fat}}} \tag{26}$$

and $f_{ck,fat}$ is the concrete fatigue strength. These expressions can be considered valid for concrete stored in a constant environment of approximately 20^oC, 65% RH. The curves have been verified with experiments up to 10^7 load cycles to failure. For $\log N > 8$ the curves asymptotically approach the minimum stress level of the respective curve. In the fib Model Code 2010 [12], the fatigue reference compressive strength $f_{ck,fat}$ is obtained from the characteristic compressive strength f_{ck} as follows:

$$f_{ck,\text{fat}} = 0.85\alpha_{cc}(t)\left[f_{ck}\left(1 - \frac{f_{ck}}{25f_{ck0}}\right)\right] \tag{27}$$

with $\alpha_{cc}(t)$ is given by Equation (28) and $f_{ck0} = 10\text{MPa}$.

$$\alpha_{cc}(t) = \exp\left\{s\left[1 - \left(\frac{28}{t}\right)^{0.5}\right]\right\} \tag{28}$$

The expression for $\beta_{cc}(t)$ describes the strength evolution with time, where s depends on the strength class of the cement, see [12].

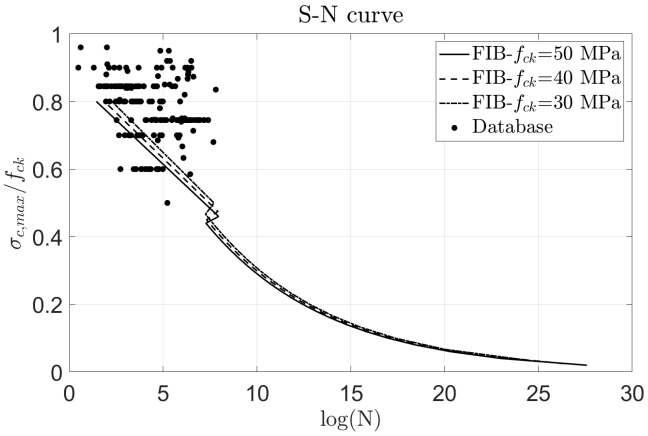

Figure 4: Comparison between the experimental data and the S-N curves from the FIB Model Code 2010.

Figure 4 plots the experimental data used for calibration and the S-N curves from Eqs.22-23. The plots prove that the Fib Model is highly conservative, being almost the lower envelope of the test data. Therefore, it cannot be used for fitting purposes, as discussed in the next sections. Even if the Fib Model is unbiased, the fitting is still unsatisfactory, making it unsuitable for predictions. Additionally, the model is deterministic and does not allow estimating the failure probability due to fatigue.

4.3. Proposed model and discussion

The proposed probabilistic fatigue model, derived from the step-wise deletion can be written as:

$$\log\left[C\left(\mathbf{x},\boldsymbol{\Theta}\right)\right] = \log\left[\hat{C}\left(\mathbf{x}\right)\right] + \boldsymbol{\theta}\boldsymbol{h} + \sigma\varepsilon \tag{29}$$

where $\boldsymbol{\theta}$ and $\boldsymbol{h}$ are defined in Table C.9. The θ_i are identified by the subscripts corresponding to the combinations of the i, j and z coefficients of Equation (16). The posterior statistics of $\boldsymbol{\Theta}$ is reported in Table C.9. Figure 5 plots the steps of the model deletion process. The left y-axis in the logarithmic scale shows the coefficient of variations of the θ_i considered at the i-th step. The right y-axis plots the standard deviation of the model error σ. The initial number of coefficients, obtained from Equation (16), is equal to 64. The high number of regressors can be associated with overfitting issues. Therefore, to test the absence of overfitting, the dataset in Table 2

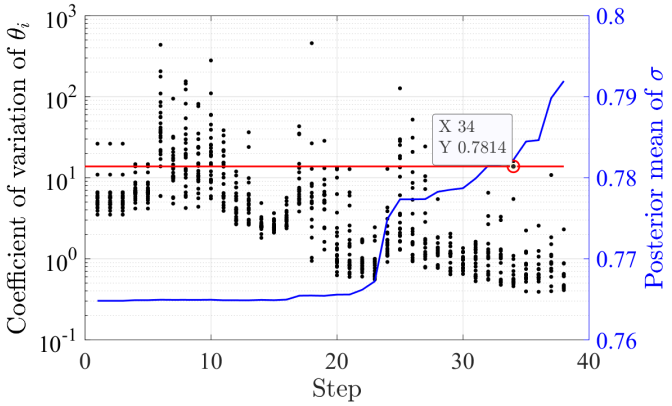

Figure 5: Step-wise model deletion.

has been divided into two subsets, for calibration and validation purposes, respectively. The calibration set includes 80% of the data, while the test set has the remaining 20%.

The model calibration with all terms leads to a σ equal to 0.76 until the 23rd step. At this step, the model error has a significant increment until stabilizing at 0.78. The further reduction of the model error leads to a standard deviation close to 0.9-1, observed in the linear model. Therefore, the authors chose the 34th step for model truncation for two reasons. Further steps lead to a significant increment of the model error, which would become close to the one in the first-order model, thus impairing the advantages of the more advanced formulation. Secondarily, the 34th step is not associated with overfitting, as proved by the good agreement between the fitting of the calibration set and the data set. Therefore, the selected model possesses 20 explanatory functions, itemized in Table C.9. The discussion of the model performance is carried out by comparing it with the predictions of a first-order one, shown in Equation (30), and a modification of the deterministic model in Equation (31) to eliminate the bias in the estimates.

$$\log\left[C\left(\mathbf{r},\hat{\mathbf{s}},\boldsymbol{\Theta}\right)\right] = \theta_{000} + \theta_{100}h_{100} + \theta_{010}h_{010} + \theta_{001}h_{001} + \sigma\varepsilon \tag{30}$$

$$\log\left[C\left(\mathbf{r},\hat{\mathbf{s}},\boldsymbol{\Theta}\right)\right] = \log\left[\hat{C}\left(\mathbf{r},\hat{\mathbf{s}},\boldsymbol{\Theta}\right)\right] + \theta_{000} + \sigma\varepsilon \tag{31}$$

Table 2 compares the performances of the first-order model in Equation (30), the unbiased Fib Model in Equation (31) and the proposed one. The standard deviation of the model error reduces from the Fib Model to the first-order and

Table 2: Comparison between predictive models, where σ is the standard deviation.

Models	σ	R^2	adj-R^2
First-order Model	1.230	0.409	0.401
Fib Model	1.580	0.023	0.018
Proposed model	0.781	0.818	0.788

the proposed one, being nearly 1.5, 1.2 and 0.8, respectively. As highlighted by [41], concrete fatigue evidence a highly scattered response. Therefore, it is not possible to further reduce the modelling error due to the significant fraction of σ related to the dataset, which is irreducible.

The ranking between the three models in terms of R^2 and adj-R^2 is more evident. The first-order model has an R^2 close to 0.4. On the other hand, the R^2 of the Fib-model is extremely low, nearly about 0.023. Conversely, the proposed model has a satisfactory R^2, approximately equal to 0.8. Figure 6

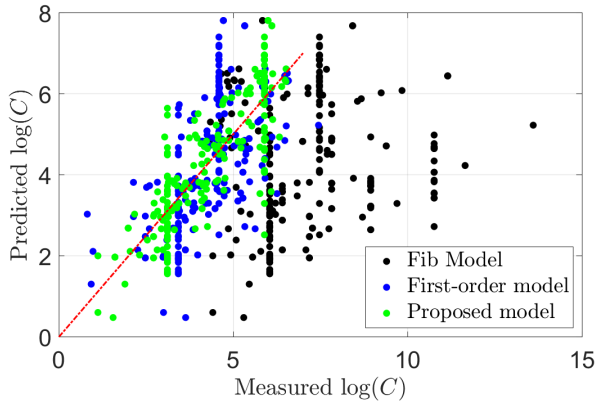

Figure 6: Predicted versus the measured number of cycles to failure for the Fib model, the first-order and the proposed ones.

compares the performances of the three models by plotting the logarithms of the number of cycles to failure estimated from the model and those taken from the dataset. Figure 6 also plots the bisector of the first quadrant. The higher is the distance from the 1:1 line, the worse the model performance. The first-order and the proposed model appear quite close to the 1:1 line. Conversely, the dots of the fib model do not align along the bisector. Instead, they are likely to arrange along a line with a lower slope than the bisector. This fact proves the estimated low value for the R^2 in Table 2. Additionally,

it suggests that the elementary correction of the Fib model in Equation (31) is not enough to achieve a suitable fitting. Therefore, a more sophisticated model should be used for predictions like the one proposed in this paper.

5. Parametric fragility curves

This section shows a selection of fragility curves related to fatigue failure. The parameters varied in these analyses are:

- The maximum stress level ($S_{c,max}$), see Figure 7 and Table 3;
- The number of expected trains per day ($n_{t,d}$), see Figs.7-9 and Tabs.3-5;
- The standard deviation of the fatigue model (σ), see Figure 8 and Table 4;
- The train velocity (c), see Figure 9 and Table 5.

The stress levels are assumed in the calculations, and they are not obtained from a specific structure by solving the TTBI equations. Therefore, the fragility curves are general and can refer to any structure theoretically. Three values for the expected number of trains per day have been assumed: 40, 100 and 150. These values derive from the classification of the Italian railway network, based on small ($n_t < 40$), moderate ($40 < n_t < 100$) or high traffic ($n_t > 100$).

The effect of the train velocity is specific to the structure. Therefore, the authors used the amplification factor for the stress level obtained from the case study discussed in the following sections to estimate velocity effects. Two standard deviations for the fatigue model are considered, one equal to 0.78 from the proposed model, while another equal to 1.5 arising from the Fib Model. Figure 7 plots the estimated failure probabilities as a function of the number of years, chosen as intensity measure. The four plots refer to a maximum stress level equal to 0.1, 0.15, 0.2 and 0.25. Each figure shows three fragility curves associated with the considered traffic demand levels, 40, 100 and 150 trains per day. The parameters assumed constant in the calculations are the concrete compression strength f_{ck}=45, the minimum stress level ($S_{c,min} = 0.01$), the train velocity ($c = 100$km/h) and the standard deviation of the fatigue model ($\sigma = 0.78$). These values are also reported in the title of each figure to facilitate the reader.

Figure 7 shows the mean of the fragility curves. The direct inspection of Figure 7 proves the followings:

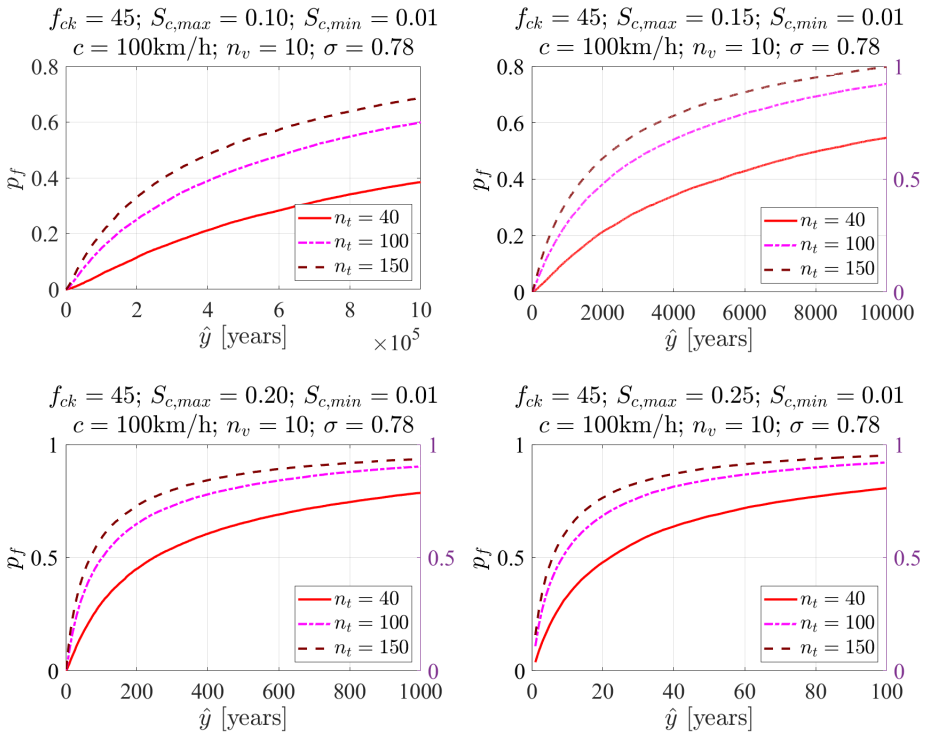

Figure 7: Fragility curves (left y-axis) and reliability indexes (right y-axis) for railway concrete bridges with variable stress level and train traffic by assuming $f_{ck} = 45$, $S_{c,min} = 0.01$, c= $100km/h$, $n_v = 10$. The standard deviation of the fatigue model (σ) is assumed equal to 0.78.

- The fragility curves do not reach values close to 1 also for significant intensity measures. This fact depends on the high uncertainty of the fatigue model. Parallelly, the curves collecting the reliability indexes prove that the reliability index can be very low for minimal intensity measures.

- The train traffic reduces structural reliability. However, the effect of the stress level is enormously more significant than that of the train traffic, in the considered ranges of variation.

- There is a sharp reduction of the structural reliability between maximum stress levels between 0.1 and 0.25. If the stress level is lower than 0.1, fatigue cracking is unlikely to occur. Conversely, a 10% increment of the stress level causes a boost in the failure probability due to fatigue. Consequently, the fatigue model and the fragility curves are highly sensitive to stress levels.

Table 3: Estimated fatigue life in years ($\hat{n}_y$) and associated standard deviation (σ_y) for railway concrete bridges with variable stress level and train traffic by assuming $f_{ck} = 45$, $S_{c,min} = 0.01$, c= $100km/h$, $n_v = 10$. The standard deviation of the fatigue model (σ) is assumed equal to 0.78.

Expected	Expected number of trains per day ($n_{t,d}$)					
stress level	40		100		150	
$S_{c,max}$	$\hat{n}_y$	σ_y	$\hat{n}_y$	σ_y	$\hat{n}_y$	σ_y
0.1	30358	7334	12687	2107	7855	1671
0.15	140	28	56	11	44	6
0.2	5	1	2	/	1	/
0.25	<1	/	<1	/	<1	/

Table 3 lists the estimated fatigue lives for the curves in Figure 7. The fatigue life reduces dramatically for $S_{c,max}$ between 0.1 and 0.25. Higher values of fatigue life are associated with higher uncertainty in the estimate, expressed in terms of standard deviation. The accurate estimate of the stress level inside a structure is crucial for predicting the fatigue life, and, accordingly scheduling the inspections for assessing the integrity of concrete (sonic tests, e.g.). Figure 8 shows the same calculations plotted in Figure 7 by adopting a higher standard deviation for the fatigue model (σ=1.5). The uncertainty of the fatigue model does not provide an adequate estimate of

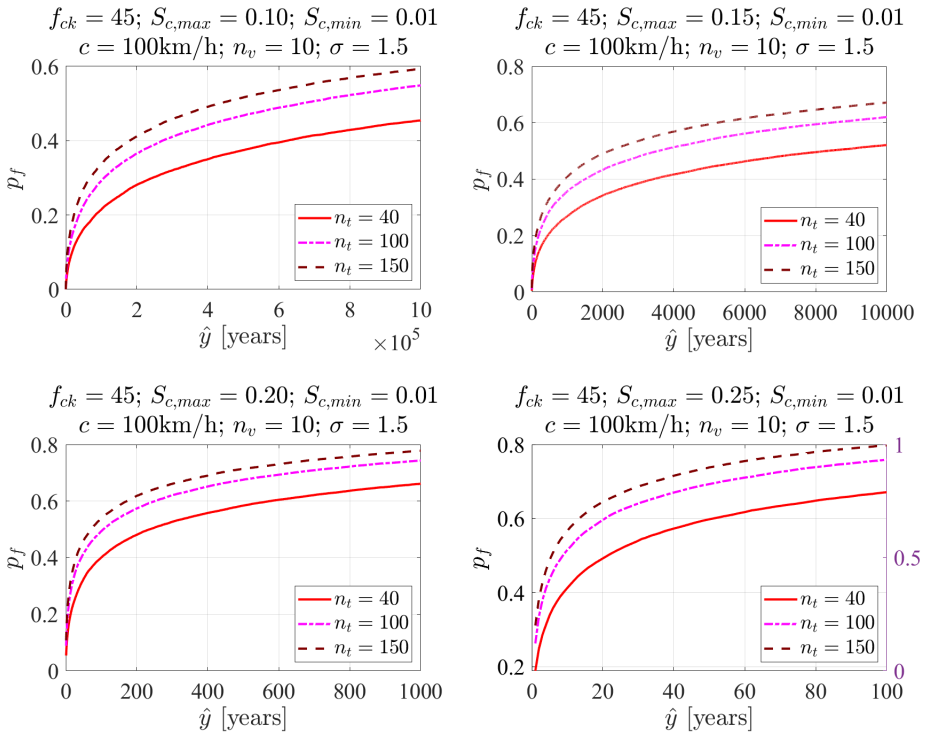

Figure 8: Fragility curves (left y-axis) and reliability indexes (right y-axis) for railway concrete bridges with variable stress level and train traffic by assuming $f_{ck} = 45$, $S_{c,min} = 0.01$, c= $100km/h$, $n_v = 10$. The standard deviation of the fatigue model (σ) is assumed equal to 1.5, as in the Fib Model.

the fragility curves. The failure probability is very low, despite considering high-intensity measures. Parallelly, except for $S_{c,max} = 0.1$, the reliability indexes are far below 4 for $\hat{y} < 1$. Table 4 confirms the above aspects. If the

Table 4: Estimated fatigue life in years ($\hat{n}_y$) and associated standard deviation (σ_y) for railway concrete bridges with variable stress level and train traffic by assuming $f_{ck} = 45$, $S_{c,min} = 0.01$, c= $100km/h$, $n_v = 10$. The standard deviation of the fatigue model (σ) is assumed equal to 1.5.

Expected	Expected number of trains per day (n_t)					
stress level	40		100		150	
$S_{c,max}$	$\hat{n}_y$	σ_y	$\hat{n}_y$	σ_y	$\hat{n}_y$	σ_y
0.1	620	216	227	92	155	60
0.15	3	1	1	<1	1	<1
0.2	<1	/	<1	/	<1	/
0.25	<1	/	<1	/	<1	/

stress level is higher than 0.1, the expected fatigue life is always lower than 1 year.

Figure 9 plots the fragility curves by varying the expected train traffic and the train velocity. As anticipated, the results of these plots cannot be considered general since the stress amplification due to velocity has been obtained from the TTBI model for the case study discussed in the following sections. However, the considered bridge represents a typical short-span reinforced concrete railway bridge. Therefore, the results can be considered valid for a variety of situations. The calculations in Figure 9 refer to a maximum stress level equal to 0.2. The estimated fatigue lives in years, shown in Table 5, confirm that the effect of velocity are minor compared to those caused by the train traffic and the stress level. In conclusion, the ranking of the parameters from the most to the least influential to the fatigue life is: stress level, train traffic and train velocity.

6. Case study

The authors estimate the fragility curves and the fatigue life for a short-span prestressed concrete railway bridge. The bridge in Figure 10 is on the Orte-Falconara railway line, in the municipality of Trevi (Italy). The viaduct consists of 46 spans of about 20 m in length. Each span consists of 8 pre-tensioned beams equipped with four crosspieces with rectangular

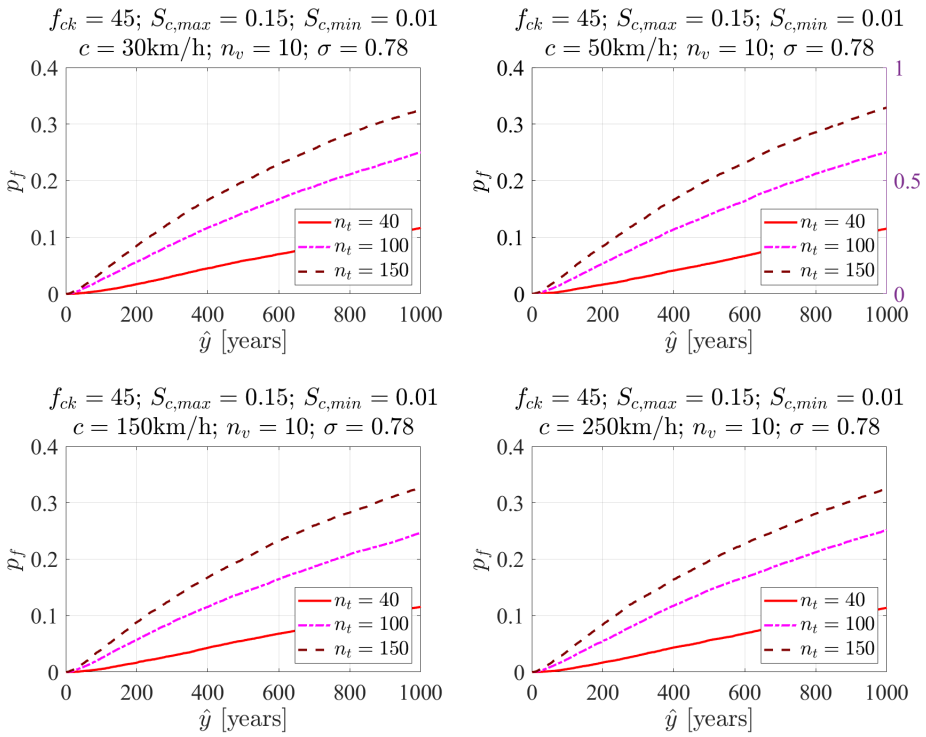

Figure 9: Fragility curves (left y-axis) and reliability indexes (right y-axis) for railway concrete bridges with variable train velocity c and train traffic by assuming $f_{ck} = 45$, $S_{c,min} = 0.01$, $S_{c,min} = 0.2$, $n_v = 10$. The standard deviation of the fatigue model (σ) is assumed equal to 0.78 based on the proposed fatigue model.

Table 5: Estimated fatigue life in years ($\hat{n}_y$) and associated standard deviation (σ_y) for railway concrete bridges with variable train velocity c and train traffic by assuming $f_{ck} = 45$, $S_{c,min} = 0.01$, $S_{c,min} = 0.2$, $n_v = 10$. The standard deviation of the fatigue model (σ) is assumed equal to 0.78 based on the proposed fatigue model.

Train	Expected number of trains per day (n_t)					
velocity	40		100		150	
c [km/h]	$\hat{n}_y$	σ_y	$\hat{n}_y$	σ_y	$\hat{n}_y$	σ_y
30	140	38	60	12	38	8
50	163	28	54	13	42	6
150	139	29	56	11	40	9
250	148	26	59	9	39	8

cross-sections. The bridge is not particularly sensitive to fatigue under compression since the stress ratio is not as significant as in other structures, like multi-span continuous bridges, with slender members. However, this case study represents an application of the above procedure for assessing fatigue in an ordinary prestressed concrete structure, which is a dominant mid-span bridge typology in railway networks. This case study is particularly significant because it shows that, despite the relatively low-stress ratio, the fatigue life is insufficient, being shorter than the structural life. As later commented, the consequence of the high uncertainty of the fatigue model is the reduction of the fatigue life. The considered fatigue failure mode corresponds to eccentric compression. The fatigue failure is expected to appear by the bridge mid-span, where the maximum stress ratios should appear in the case of a simply-supported bridge considered in this investigation.

Figure 10: Views of the viaduct and of a sample span.

Figure 11 details the cross-section of each span. The beams are 1.40 m high. The upper and lower wings are 1.20 m and 0.70 m wide, respectively. The eight beams have a shear reinforcement by the supports. Therefore the thickness of the core of the beam varies from 16 to 33cm. The prestressing reinforcement is arranged in the lower wing, and, according to the design drawings of the time, it consists of 29 cables arranged in 3 rows, sheathed at the support. The crosspieces are also prefabricated and are therefore born integral with the beam. They have a rectangular cross-section with a 40cm width and a height equal to the beams. There is a 20 cm thick reinforced concrete slab with 1.40 cantilevered elements, which support the side walkways to the railway line and the parapets. The total width of the deck is about 12.40 m and bears two running tracks. Table 6 lists the geometrical characteristics of the bridge cross-section.

6.1. Experimental tests and model calibration

The displacement response of the bridge under a train transit is used to calibrate the parameters of the FD model. The experimental equipment

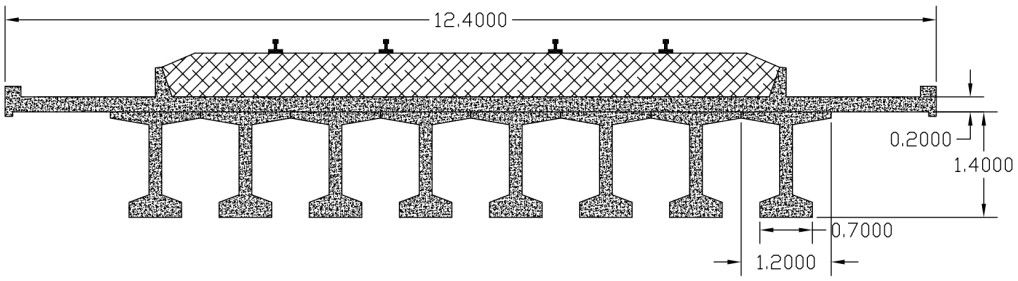

Figure 11: Cross-section of the Orte-Falconara bridge. The dimensions are in meters.

consisted of two easels supporting a laser sensor. The laser sensors are Micro-epsilon optoNCDT 1420. The sampling rate is 1000Hz. The C-Box/2A controller (Micro-epsilon) synchronizes and digitizes the two signals, which are acquired by a personal computer from an Ethernet cable. A lead-acid battery provided power to both the laser sensors, the controller and the personal computer. The two lasers measured the displacement response of the 3rd and 6th beam intrados. Figure 12 shows the experimental setup for the Orte-Falconara bridge.

Figure 12: View of the sensors layout and experimental setup in the Orte-Falconara bridge (1st case study) for the bridge deflection measurement using laser sensors under the train transit.

The train loads are eccentric and cause minor torsional effects. Since the authors are modelling the bridge like an EB beam, they purged the response from the torsional response by extracting the mean value, also shown in Figure 13.

As proven by [27], under eccentric compressive tests, the strains on cross sections keep nearly perfect linear distributions. Therefore, the EB model

can be considered reasonable since it assumes the planarity of the cross-section deformation. Besides, as recently highlighted by [4], the modelling of the ballast contribution is particularly relevant when estimating the load effect of the bridge. Therefore, the authors developed a TTBI model where the bridge and the rail are modelled by EB beams coupled with a layer of springs representing the ballast. Additionally, the choice of an analytical rather than a Finite Element model relies on the computational cost. Rapid analyses to calculate the empirical fragilities demand a particularly efficient structural model. The main limitation of the model is neglecting the effect of load eccentricity on stress redistribution among the eight longitudinal beams. Therefore, future studies will be based on more accurate structural models than the archetypal one used in this paper.

Following [4], the experimental time history is used to calibrate the stiffness and damping parameters of TTBI model (EI_b, k_f, c_f). The known parameters are listed in Table 6. The calibration is carried out using a genetic optimization algorithm [11]. The genetic algorithm performs iteration of parameters with the goal of minimizing the following objective function: The optimum parameters are defined as:

$$\hat{\boldsymbol{X}} = \arg\min_{\boldsymbol{X}} \operatorname{corr}(\boldsymbol{d}_{s,s}, \boldsymbol{d}_{s,m}) \tag{32}$$

$$\operatorname{obj}(\mathbf{p}) = \frac{\sum_{i=1}^{N} |\left[w_{b,ei} - w_{b,si}(\mathbf{p})\right] \Delta t_i|}{\sum_{i=1}^{N} |w_{b,ei} \Delta t_i|} \tag{33}$$

where N is the number of data points, $\mathbf{p}$ is the parameter vector containing the ballasted track parameters, $w_{b,ei}$ and Δt_i are the experimental deflection of the bridge, and $w_{si}(\mathbf{p})$ is the simulated beam deflection. Note that the objective function is defined as the normalized integral of the difference between experimental and simulated displacement. This gives a measure of the discrepancy between experimental data and model simulation.

$$\boldsymbol{p} = \{EI_b, k_f, c_f\} = \{12600\,\mathrm{kN}\cdot\mathrm{mm}^2,\ 490.49\,\mathrm{MPa}, 14.50\,\mathrm{MPa}\cdot s\} \tag{34}$$

Equation (34) gives the optimum parameters, while Figure 13 compares the experimental and simulated displacement response. The comparison is very satisfactory. The displacement peaks are almost corresponding. Additionally, the oscillations damp after each train load, as observed in the experimental data. Therefore, the calibrated FD model can be reliably used to predict the stress level inside the bridge.

Table 6: Input parameters of the optimization algorithm.

Input parameters			
Description	Label	Value	Unit
Beam length	L	19.85	m
Discretization step	Δx	0.5	m
Concrete specific mass	ρ_c	2500	kg/m^3
Cross-section area of the bridge	A_c	6.67	m^2
Ballast specific mass	ρ_b	2000	kg/m^3
Cross-section area of the rails	A_r	0.01	m^2
Steel specific mass	ρ_s	2000	kg/m^3
Cross-section area of the ballast	A_b	5.67	m^2
Bending stiffness of the bridge	E_cI_c	12600	kN·mm^2
Young's modulus of steel	E_s	210000	Mpa
Cross section area of the rails	I_r	833·10^4	mm^4
Velocity of the train	c	110	km/h
Locomotive's length	L_v	5	m
Car's length	L_v	22	m
Locomotive weight	P_l	300	kN
Car's weight	P_c	600	kN
Number of locomotives		2	
Number of cars		7	
Train velocity	c	109	km/h

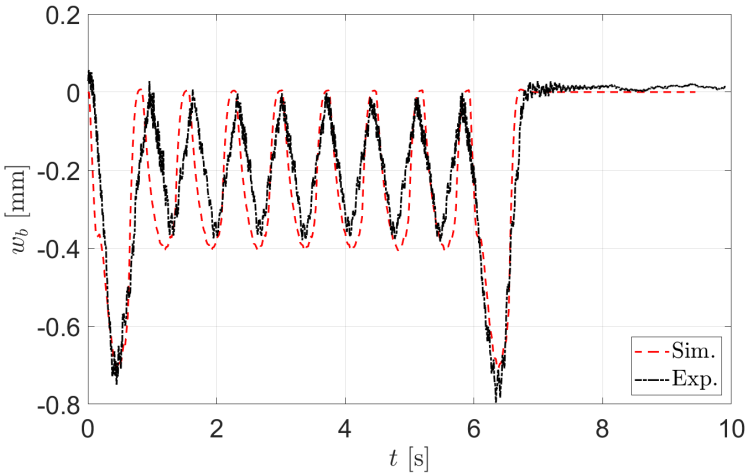

Figure 13: Comparison between the experimental and simulated displacement response obtained with the optimized parameters.

6.2. Demand model

The demand model in Equation (6) is estimated from the 2017-2021 database collecting the information of the trains that crossed the considered bridge. Figure 14 shows the histogram plots of the most relevant information referred to in 2017 in terms of train weight, length, number of vehicles and velocity. The values cannot be approximated by continuous probability density functions, as proven by attempting a fitting of the weight, length and vehicles using a Weibull probability distribution. A single train transit, as later shown, will be used for calibrating the train-track bridge interaction model. Conversely, the database corresponding to the trains passed in 2017 is used for estimating the demand model related to a given year following Equation (6).

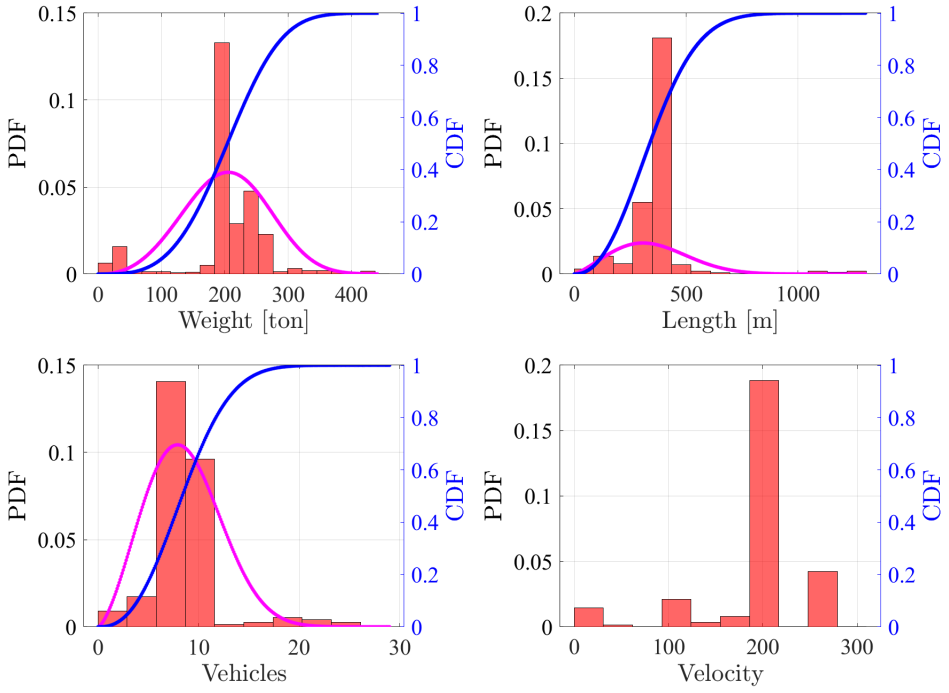

Figure 14: Histogram plot and fitting Weibull probability distributions of the main information about the train transits in 2017.

The information collected in the database has been correlated in Figure 15 to show the dependence between the axis weight and the number of axes (Figure 15(a)) and the axes weight and the number of cycles per year

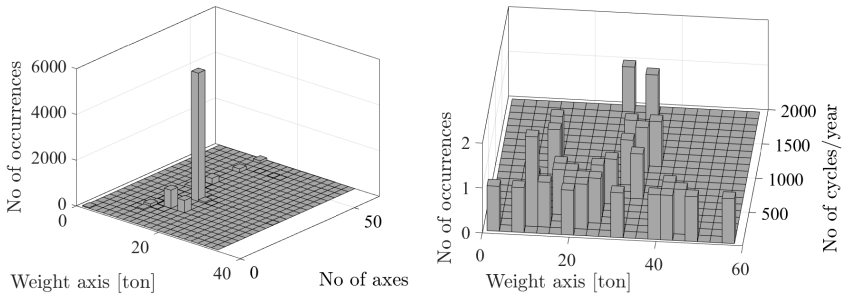

Figure 15: Histogram plot of the number of axes/axes weight and number of cycles per year/axes weight data.

(Figure 15(b)). Figure 15(a) proves that, in most cases, there are 25 axes with an approximate 20ton weight. However, the are multiple situations where different axes weights are associated with a very different number of cycles per year. This fact endorses the use of the discrete model in Equation (6) based on the database of train traffic.

7. Fatigue life assessment

Figure 16 shows the fragility curves for the considered bridge in Figure 10. It plots the estimated failure probabilities as a function of the number of years, chosen as the intensity measure. The two figures have been obtained by varying the standard deviation of the fatigue model, set equal to 0.78 and 1.5 following the above calculations. The reference stress levels used for normalization are $\boldsymbol{s} = \{S_{c,max}, S_{c,min}\} = \{0.01, 0.18\}$ Therefore, the parameters assumed constant in the calculations are the concrete compression strength f_{ck}=45, and the standard deviation of the fatigue model ($\sigma = 0.78$). These values are also reported in the title of each figure to facilitate the reader. Figure 16(c)-(d) shows the same results in (a)-(b) using the number of cycles as intensity measure. Table 7 lists the estimated fatigue life by assuming the

Table 7: Estimated fatigue life in years ($\hat{n}_y$) and associated standard deviation (σ_y) for the considered case study bridge by assuming two values for the standard deviation of the fatigue model.

σ	$\hat{n}_y$	σ_y
0.78	10	2
1.5	1	<1

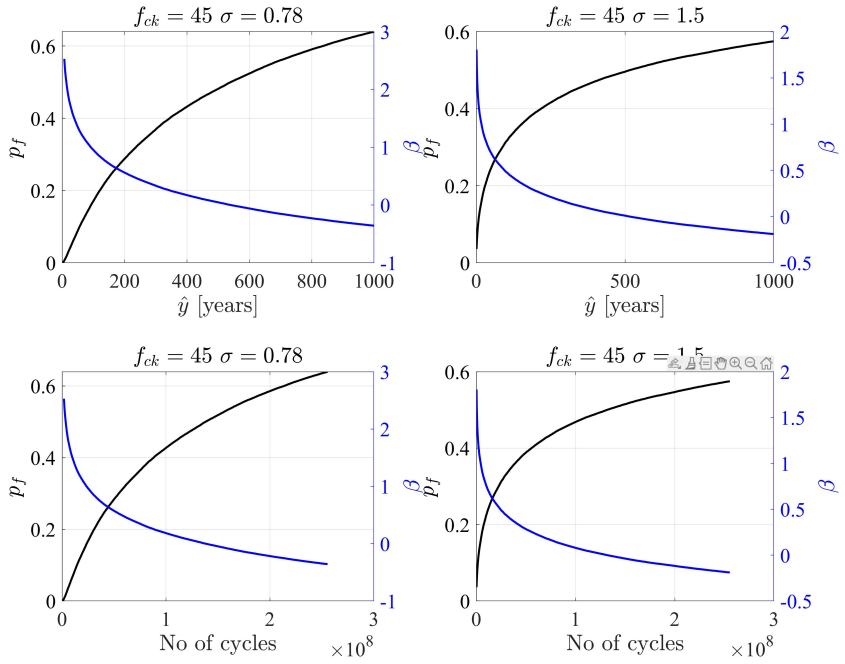

Figure 16: Fragility curves (left y-axis) and reliability indexes (right y-axis) for the considered case study, by assuming two standard deviations for the fatigue model (σ) corresponding to the proposed one (a) and the Fib Model (b). The plots in (c) and (d) correspond to the ones in (a) and (b) where the intensity measure is the number of cycles.

two standard deviations. According to the proposed model, the fatigue life equals ten years with a two-year standard deviation. Conversely, the fatigue life obtained with $\sigma = 1.5$ is equal to 1 year. The above results highlight the following aspect. If the stress level ($S_{c,max}$) exceeds the asymptote 0.1, the fatigue life is far below the nominal life of a railway concrete bridge. This is also valid if the proposed fatigue model with a lower standard deviation is used. Therefore, the evaluation of the stress level inside a concrete bridge should be as accurate as possible since the fatigue life is extremely sensitive to the stress level.

The proposed fatigue life assessment can be used to schedule in-depth tests to check the integrity of concrete structures. Additionally, structural health monitoring systems for concrete bridges subjected to repetitive loadings, like railway bridges, should include adequate sensing solutions for the continuous tests of the concrete integrity. The fatigue damage can trigger dangerous phenomena which can lead to a significant reduction of structural reliability. Therefore, this model can support more efficient maintenance planning and management savings related to cost savings and lifetime extensions.

8. Conclusions

This paper proposes a general probabilistic framework for estimating the fatigue life of concrete structures applied to prestressed concrete railway bridges. The proposed approach is general and can be applied to other engineering problems, such as the fatigue degradation of wind power plants under wind actions. The fatigue life is obtained from the empirical estimates of the fragility curves following a direct Montecarlo approach and a homogenization strategy based on S-N curves. The fragility curves plot the failure probability as a function of the number of years chosen as the intensity measure for the fragility estimate. Failure is reached when the number of cycles obtained from the demand model at a given year exceeds the number of cycles to failure obtained from a probabilistic fatigue model. The paper highlights the limits of available fatigue models, which are deterministic and affected by a high modelling error when fitting experimental data.

Following [32], the authors used a database of fatigue tests on normal-strength concrete samples to calibrate a probabilistic capacity model. The proposed model, calibrated following a Bayesian approach, exhibits a good fitting of the experimental data with R^2 approximately equal to 0.8. However,

it is impossible to reduce the standard deviation below 0.8 without overfitting issues. The fatigue model is obtained by correcting the Fib Model 2010 with 30 regressors, selected following a model deletion process based on the coefficient of variation values [21]. The demand model used for predicting the number of load cycles per year is obtained from a homogenization approach by uniforming the number of cycles to the stress level using the probabilistic fatigue model. The stress level inside the structure is estimated from an analytical train-track-bridge interaction model, calibrated on experimental data.

The entire procedure is applied to derive fragility curves in general cases by varying the stress level, the train traffic, the train velocity and the fatigue model uncertainty. The significant uncertainty of the fatigue response significantly reduces the expected fatigue life. If the stress level ($S_{c,max}$) exceeds the asymptote 0.1, the fatigue life is far below the expected lifetime of a concrete railway bridge. This result is also valid if the proposed fatigue model with a lower standard deviation is used. The train traffic reduces structural reliability. However, the effect of the stress level is enormously more significant than that of the train traffic in the considered ranges of variation. Therefore, the evaluation of the stress level inside a concrete bridge should be as accurate as possible since the fatigue life is extremely sensitive to the stress level.

The fatigue damage can trigger dangerous phenomena, leading to a significant reduction of structural reliability. Therefore, the proposed fatigue life assessment can be used to schedule in-depth tests to check the integrity of concrete structures. Fatigue's contribution to the cracking of concrete railway bridges is very hard to quantify. So it is difficult to get the real fatigue failure cycles in actual bridges. The main model limitation originates from this observation. Accordingly, the model has never been validated against the fatigue collapse of real bridges. Future studies will consider other fatigue-related failure modes in reinforced concrete structures, such as fatigue of the steel rebars and concrete fatigue in tension.

9. Data Availability Statement

All data, models, or code that support the findings of this study are available from the corresponding author upon reasonable request.

References

[1] Aarthi, K., Arunachalam, K., and Thivakar, S. (2016). A probabilistic fatigue failure analysis for frscc with granite sawing waste. *Computers and Concrete*, 18(5):969–982.

[2] Aloisio, A., Contento, A., Alaggio, R., Briseghella, B., and Fragiacomo, M. (2022a). Probabilistic assessment of a light-timber frame shear wall with variable pinching under repeated earthquakes. *Journal of Structural Engineering*, 148(11):04022178.

[3] Aloisio, A., Contento, A., Boggian, F., and Tomasi, R. (2023a). Probabilistic friction model for aluminium–steel asymmetric friction connections (afc). *Engineering Structures*, 274:115159.

[4] Aloisio, A., Rosso, M. M., and Alaggio, R. (2022b). Experimental and analytical investigation into the effect of ballasted track on the dynamic response of railway bridges under moving loads. *Journal of Bridge Engineering*, 27(10):04022085.

[5] Aloisio, A., Ussher, E., Fragiacomo, M., and Tomasi, R. (2023b). Capacity models for timber under compression perpendicular to grain with screw reinforcement. *European Journal of Wood and Wood Products*, pages 1–22.

[6] Baktheer, A. and Chudoba, R. (2021). Experimental and theoretical evidence for the load sequence effect in the compressive fatigue behavior of concrete. *Materials and Structures*, 54(2):1–23.

[7] Bazant, Z. P. and Hubler, M. H. (2014). Theory of cyclic creep of concrete based on paris law for fatigue growth of subcritical microcracks. *Journal of the Mechanics and Physics of Solids*, 63:187–200.

[8] Box, G. E. and Tiao, G. C. (1992). *Bayesian Inference in Statistical Analysis*. John Wiley & Sons, Ltd.

[9] Casas, J. R. (2009). A probabilistic fatigue strength model for brick masonry under compression. *Construction and Building Materials*, 23(8):2964–2972.

[10] Castillo, E. and Fernández-Canteli, A. (2009). *A unified statistical methodology for modeling fatigue damage*. Springer Science & Business Media.

[11] Chipperfield, A., Fleming, P., Pohlheim, H., and Fonseca, C. (1994). A genetic algorithm toolbox for matlab. In *Proc. International Conference on Systems Engineering, Coventry, UK*, volume 6.

[12] Code, F. M. (2012). International federation for structural concrete (fib): Lausanne.

[13] Contento, A., Aloisio, A., Xue, J., Quaranta, G., Briseghella, B., and Gardoni, P. (2022). Probabilistic axial capacity model for concrete-filled steel tubes accounting for load eccentricity and debonding. *Engineering Structures*, 268:114730.

[14] Craig Jr, R. R. and Kurdila, A. J. (2006). *Fundamentals of structural dynamics*. John Wiley & Sons.

[15] Di Lorenzo, S., Di Paola, M., Failla, G., and Pirrotta, A. (2017). On the moving load problem in euler–bernoulli uniform beams with viscoelastic supports and joints. *Acta Mechanica*, 228(3):805–821.

[16] Dormand, J. R. and Prince, P. J. (1980). A family of embedded runge-kutta formulae. *Journal of computational and applied mathematics*, 6(1):19–26.

[17] Dyduch, K., Szerszeń, M., and Destrebecq, J.-F. (1994). Experimental investigation of the fatigue strength of plain concrete under high compressive loading. *Materials and Structures*, 27(9):505–509.

[18] Fehling, E., Schmidt, M., Teichmann, T., Bunje, K., Bornemann, R., and Middendorf, B. (2005). *Entwicklung, Dauerhaftigkeit und Berechnung ultrahochfester Betone (UHPC): Forschungsbericht DFG FE 497/1-1*. kassel university press Kassel, Germany.

[19] Feng, D. and Feng, M. Q. (2015). Model updating of railway bridge using in situ dynamic displacement measurement under trainloads. *Journal of Bridge Engineering*, 20(12):04015019.

[20] Frỳba, L. (2013). *Vibration of solids and structures under moving loads*, volume 1. Springer Science & Business Media.

[21] Gardoni, P., Der Kiureghian, A., and Mosalam, K. (2002). Probabilistic capacity models and fragility estimates for rc columns based on experimental observations. *ASCE Journal of Engineering Mechanics*, 128(10):1024–1038.

[22] Gaspar, R. and Stucchi, F. R. (2013). Web design of box girders concrete bridges. *Engineering structures*, 57:267–275.

[23] Holmen, J. O. (1982). Fatigue of concrete by constant and variable amplitude loading. *Special Publication*, 75:71–110.

[24] Hordijk, D., Wolsink, G., and De Vries, J. (1995). Fracture and fatigue behaviour of a high strength limestone concrete as compared to gravel concrete. *HERON-ENGLISH EDITION-*, 40:125–146.

[25] Hsu, T. T. (1981). Fatigue of plain concrete. In *Journal Proceedings*, volume 78, pages 292–305.

[26] Jiang, C., Gu, X., Huang, Q., and Zhang, W. (2017a). Deformation of concrete under high-cycle fatigue loads in uniaxial and eccentric compression. *Construction and Building Materials*, 141:379–392.

[27] Jiang, C., Huang, Q., Gu, X., and Zhang, W. (2017b). Experimental investigation on carbonation in fatigue-damaged concrete. *Cement and Concrete Research*, 99:38–52.

[28] Ju, S.-H., Lin, H.-T., and Huang, J.-Y. (2009). Dominant frequencies of train-induced vibrations. *Journal of Sound and Vibration*, 319(1-2):247–259.

[29] Kim, J., Yi, C., Lee, S.-J., and Zi, G. (2013). Flexural fatigue behaviour of concrete under uniaxial and biaxial stress. *Magazine of concrete research*, 65(12):757–764.

[30] Klausen, D. (1978). *Strength and damage of concrete after repeated stress cycles*. PhD thesis, PhD thesis, Darmstadt, Geramny: Technische Hochschule Darmstadt.(in German).

[31] Kwon, K. and Frangopol, D. M. (2010). Bridge fatigue reliability assessment using probability density functions of equivalent stress range based on field monitoring data. *International journal of fatigue*, 32(8):1221–1232.

[32] Lantsoght, E. O., van der Veen, C., and de Boer, A. (2016). Proposal for the fatigue strength of concrete under cycles of compression. *Construction and Building Materials*, 107:138–156.

[33] Li, Z., Chan, T., and Ko, J. (2002). Determination of effective stress range and its application on fatigue stress assessment of existing bridges. *International Journal of Solids and Structures*, 39(9):2401–2417.

[34] Lohaus, L. and Anders, S. (2007). High-cycle fatigue of "ultra-high performance concrete" and "grouted joints" for offshore wind energy turbines. In *Wind Energy*, pages 309–312. Springer.

[35] Lohaus, L., Oneschkow, N., and Wefer, M. (2012). Design model for the fatigue behaviour of normal-strength, high-strength and ultra-high-strength concrete. *Structural Concrete*, 13(3):182–192.

[36] Luo, J. and Bowen, P. (2003). A probabilistic methodology for fatigue life prediction. *Acta materialia*, 51(12):3537–3550.

[37] Mankar, A., Bayane, I., Sørensen, J. D., and Brühwiler, E. (2019). Probabilistic reliability framework for assessment of concrete fatigue of existing rc bridge deck slabs using data from monitoring. *Engineering Structures*, 201:109788.

[38] McCool, J. I. (2004). Statistical error in crack growth parameters deduced from dynamic fatigue tests. *International journal of fatigue*, 26(11):1207–1215.

[39] Nocera, F., Wang, J., Faleschini, F., Demartino, C., and Gardoni, P. (2022). Probabilistic models of concrete compressive strength and elastic modulus with rubber aggregates. *Construction and Building Materials*, 322:126145.

[40] Olsson, K. and Pettersson, J. (2010). Fatigue assessment methods for reinforced concrete bridges in eurocode. comparative study of design methods for railway bridges.

[41] Ortega, J. J., Ruiz, G., Rena, C. Y., Afanador-García, N., Tarifa, M., Poveda, E., Zhang, X., and Evangelista Jr, F. (2018). Number of tests and corresponding error in concrete fatigue. *International journal of fatigue*, 116:210–219.

[42] Owen, W. J. and Padgett, W. J. (2000). A birnbaum-saunders accelerated life model. *IEEE Transactions on Reliability*, 49(2):224–229.

[43] Palmgren, A. (1924). Die lebensdauer von kugellargern. *Zeitshrift des Vereines Duetsher Ingenieure*, 68(4):339.

[44] Paris, P. and Erdogan, F. (1963). A critical analysis of crack propagation laws.

[45] Petkovic, G., Lenschow, R., Stemland, H., and Rosseland, S. (1990). Fatigue of high-strength concrete. *Special Publication*, 121:505–526.

[46] Pimentel, M., Brühwiler, E., and Figueiras, J. (2008). Fatigue life of short-span reinforced concrete railway bridges. *Structural Concrete*, 9(4):215–222.

[47] Raju, P. R. M., Rajesh, S., Satyanarayana, B., and Ramji, K. (2012). Evaluation of stress life of aluminum alloy using reliability based approach. *International Journal of Precision Engineering and Manufacturing*, 13(3):395–400.

[48] Rao, C. and Frantz, G. C. (1995). Test on prestressed concrete bridge beams-fatigue tests of the bridge beams. Technical report.

[49] Saucedo, L., Rena, C. Y., Medeiros, A., Zhang, X., and Ruiz, G. (2013). A probabilistic fatigue model based on the initial distribution to consider frequency effect in plain and fiber reinforced concrete. *International journal of fatigue*, 48:308–318.

[50] Shah, S. P. and Chandra, S. (1970). Fracture of concrete subjected to cyclic and sustained loading. In *Journal Proceedings*, volume 67, pages 816–827.

[51] Shimizu, Y., Hirosawa, M., and Zhou, J. (2000). Statistical analysis of concrete strength in existing reinforced concrete buildings in japan. In *12th World Conference on Earthquake Engineering, Auckland, New Zealand*.

[52] Siemes, A. (1983). Fatigue of concrete, part 1: compressive stresses. Technical report, IRO-MATS/CUR report.

[53] Standard, B. (2004). Eurocode 2: Design of concrete structures—. *Part 1*, 1:230.

[54] Standard, I. (1998). General principles on reliability for structures.

[55] Stone, C. J. (1996). *A course in probability and statistics*, volume 19. Belmont: Duxbury Press.

[56] Tepfers, R. and Kutti, T. (1979). Fatigue strength of plain, ordinary, and lightweight concrete. In *Journal Proceedings*, volume 76, pages 635–652.

[57] Thai, S., Thai, H.-T., Uy, B., and Ngo, T. (2019). Concrete-filled steel tubular columns: Test database, design and calibration. *Journal of Constructional Steel Research*, 157:161–181.

[58] Tran, V.-X., Pan, J., and Pan, T. (2008). Fatigue behavior of aluminum 5754-o and 6111-t4 spot friction welds in lap-shear specimens. *International Journal of Fatigue*, 30(12):2175–2190.

[59] Walraven, J. C. et al. (2012). *Model Code 2010-Final draft: Volume 1*, volume 65. fib Fédération internationale du béton.

[60] Yuan, M., Liu, Y., Yan, D., and Liu, Y. (2019). Probabilistic fatigue life prediction for concrete bridges using bayesian inference. *Advances in structural engineering*, 22(3):765–778.

Appendix A. Train-track-bridge interaction model

Appendix A.1. Mathematical model of the track

As is well known, the deflection $w_r(x,t)$ of a track with constant mass per unit length $\rho_s A_r$, where ρ_s is the specific mass of steel and A_r is the cross-section area of the rails, and constant bending rigidity $E_s I_r$, where E_s is Young's modulus of steel and I_r is the cross-section inertia of the rails, can be described by an Euler-Bernoulli beam model. The equation of motion can be written as: [15]

$$\rho_s A_r \ddot{w}_r(x,t) + E_s I_r w_{r,xxxx}(x,t) = q_r(x,t) + f_r(x,t) \tag{A.1}$$

where the two dots, $\ddot{w}$, indicate the second time derivative of w, and $w_{r,xxxx}$ is the fourth derivative of w with respect to the spatial coordinate x. The distributed force $q_r(x,t)$ results from the viscoelastic bedding counteracting the displacement of the track:

$$q_r(x,t) = q_b(x,t) = k_f \left[w_r(x,t) - w_b(x,t)\right] + c_f \left[\dot{w}_r(x,t) - \dot{w}_b(x,t)\right] \tag{A.2}$$

where k_f and c_f represent the stiffness and damping of the viscoelastic Winkler bedding, while w_b is the deflection of the beam representing the bridge substructure. The excitation function $f_r(x,t)$ captures the effect of the interaction forces between the rails and the vehicles. The train can be modelled by a series of moving concentrated forces with identical intervals, and each car is modelled by a single concentrated force, as shown in Figure 1. Thus, a train composed of N_v cars can be considered as N_v moving forces, which are numbered as $P_k(1, 2, \ldots, N_v)$. Assuming the first force enters the bridge at the initial time, the time of the k-th load entering the bridge can be expressed as:

$$t_k = (k-1)L_v/c \tag{A.3}$$

whereL_t is full length of the train.

$$f_r(x,t) = \sum_{k=1}^{N_v} P_k \delta\left[x - c(t - t_k)\right] \tag{A.4}$$

$$P = \left\{ \frac{P_l}{2}, \left(\frac{P_l}{2} + \frac{P_c}{2} \right), P_c, \ldots, P_c, \ldots, P_c, \frac{P_c}{2} \right\} \tag{A.5}$$

where L_l is the length of the locomotive, P_k is the concentrated force related to the k-th car, P is the vector collecting all values of P_k. P_c and P_l are loads of cars and locomotives. The boundary conditions for a pinned-pinned track can be written as:

$$\text{Left boundary: } w_r(0,t) = 0 \;\; w_{r,xx}(0,t) = 0 \tag{A.6}$$

$$\text{Right boundary: } w_r(L,t) = 0 \;\; w_{r,xx}(L,t) = 0 \tag{A.7}$$

where L is the bridge length.

Appendix A.2. Mathematical model of the bridge

The bridge can be described by Euler–Bernoulli beam. The EB has a constant mass per unit length $(\rho_c A_c + \rho_b A_b)$, where ρ_c is the specific mass of concrete, A_c is the cross-section area of the beam, ρ_b is the specific mass of the ballast and A_b is the cross-section area of the ballasted track, and constant flexural rigidity $E_c I_c$, where E_c is Young's modulus of concrete and I_c the cross-section inertia of the beam. The vertical displacement $w_b(x,t)$ of the bridge is governed by the following partial differential equation [20]:

$$(\rho_c A_c + \rho_b A_b)\ddot{w}_b(x,t) + E_c I_c w_{r,xxxx}(x,t) = q_b(x,t) \tag{A.8}$$

The boundary conditions for a pinned-pinned track can be written as:

$$\text{Left boundary: } w_r(0,t) = 0 \;\; w_{r,xx}(0,t) = 0 \tag{A.9}$$

$$\text{Right boundary: } w_r(L,t) = 0 \;\; w_{r,xx}(L,t) = 0 \tag{A.10}$$

Appendix A.3. Spatial discretization

The equations of motion of the bridge–soil and the track subsystems can be written in matrix form as:

$$\begin{bmatrix} (\rho_c A_c + \rho_b A_b) & 0 \\ 0 & \rho_s A_r \end{bmatrix} \begin{Bmatrix} \ddot{w}_b(x,t) \\ \ddot{w}_r(x,t) \end{Bmatrix} + \begin{bmatrix} E_c I_c & 0 \\ 0 & E_s I_r \end{bmatrix} \begin{Bmatrix} w_{b,xxxx}(x,t) \\ \ddot{w}_{r,xxxx}(x,t) \end{Bmatrix} + \\ + \begin{bmatrix} -k_f & k_f \\ k_f & -k_f \end{bmatrix} \begin{Bmatrix} w_b(x,t) \\ w_r(x,t) \end{Bmatrix} + \begin{bmatrix} -c_f & c_f \\ c_f & -c_f \end{bmatrix} \begin{Bmatrix} \dot{w}_b(x,t) \\ \dot{w}_r(x,t) \end{Bmatrix} + \begin{Bmatrix} 0 \\ f_r \end{Bmatrix} \tag{A.11}$$

Figure 1 illustrates the mathematical model of the TTBI. The spatial discretization is obtained using the finite difference method, by approximating the fourth derivative with the approximate fourth derivative matrix. The beam is divided into n elements with a Δx length. The two coupled partial derivative equations in Equation (A.11) can be discretized into the following:

$$\begin{bmatrix} (\rho_c A_c + \rho_b A_b)\Delta x \boldsymbol{I} & \boldsymbol{0} \\ \boldsymbol{0} & \rho_s A_r \Delta x \boldsymbol{I} \end{bmatrix} \begin{Bmatrix} \ddot{\boldsymbol{w}}_b(t) \\ \ddot{\boldsymbol{w}}_r(t) \end{Bmatrix} + \begin{bmatrix} E_c I_c \boldsymbol{D}_4 - k_f \Delta x \boldsymbol{I} & k_f \Delta x \boldsymbol{I} \\ k_f \Delta x \boldsymbol{I} & E_s I_r \boldsymbol{D}_4 - k_f \Delta x \boldsymbol{I} \end{bmatrix} \begin{Bmatrix} \boldsymbol{w}_b(t) \\ \boldsymbol{w}_r(t) \end{Bmatrix} + \\ + \begin{bmatrix} -c_f \Delta x \boldsymbol{I} & c_f \Delta x \boldsymbol{I} \\ c_f \Delta x \boldsymbol{I} & -c_f \Delta x \boldsymbol{I} \end{bmatrix} \begin{Bmatrix} \dot{\boldsymbol{w}}_b(t) \\ \dot{\boldsymbol{w}}_r(t) \end{Bmatrix} + \begin{Bmatrix} 0 \\ \boldsymbol{f}_r \end{Bmatrix} = 0 \tag{A.12}$$

where $\boldsymbol{I}^{\{n\times n\}}$, $\boldsymbol{0}^{\{n\times n\}}$ are the identity and null matrices, $\boldsymbol{D}_4^{\{n\times n\}}$ is the approximate fourth matrix derivative defined in Equation (A.13), $\boldsymbol{w}_b(t)^{\{n\times 1\}}$ and $\boldsymbol{w}_r(t)^{\{n\times 1}$ collect the vertical deflection of the bridge and track models discretized in N segments, $\boldsymbol{f}_r^{\{n\times 1}$ discretizes the moving force vector described in Equation (A.1).

Matrix $\boldsymbol{D}_4^{\{n\times n\}}$ must satisfy the boundary conditions. The $\boldsymbol{D}_4^{\{n\times n\}}$ matrix is four-banded matrix. The authors imposed the boundary conditions of a

simply supported beam by replacing the coefficients in bold:

$$\boldsymbol{D}_4^{\{n\times n\}} = \frac{1}{\Delta x^4}\begin{bmatrix} \mathbf{4} & -4 & 1 & 0 & 0 & 0 & 0 & 0 & \vdots & 0 \\ \mathbf{-7/2} & 6 & -4 & 1 & 0 & 0 & 0 & 0 & \vdots & 0 \\ 1 & -4 & 6 & -4 & 1 & 0 & 0 & 0 & \vdots & 0 \\ 0 & 1 & -4 & 6 & -4 & 1 & 0 & 0 & \vdots & 0 \\ & & \ddots & \ddots & \ddots & \ddots & \ddots & & & \\ 0 & \vdots & 0 & 0 & 1 & -4 & 6 & -4 & 1 & 0 \\ 0 & \vdots & 0 & 0 & 0 & 1 & -4 & 6 & -4 & 1 \\ 0 & \vdots & 0 & 0 & 0 & 0 & 1 & -4 & -4 & \mathbf{-7/2} \\ 0 & \vdots & 0 & 0 & 0 & 0 & 0 & 1 & -4 & \mathbf{2} \end{bmatrix} \tag{A.13}$$

The bold coefficients yield a null bending moment and displacement in both the extremes of the beam.

Equation (A.12) can be re-written using the conventional notation for multi-degrees of freedom dynamic systems:

$$\boldsymbol{M}\ddot{\boldsymbol{x}}(t) + \boldsymbol{C}\dot{\boldsymbol{x}}(t) + \boldsymbol{K}\boldsymbol{x}(t) = \boldsymbol{f}(t) \tag{A.14}$$

where $\boldsymbol{M}^{\{2n\times 2n\}}$, $\boldsymbol{C}^{\{2n\times 2n\}}$ and $\boldsymbol{K}^{\{2n\times 2n\}}$ are the mass, damping and stiffness matrices, while $\boldsymbol{f}(t)$ is the forcing term. The displacement vector has the following definition: $\boldsymbol{x}^{\{2n\times 1\}} = \{\boldsymbol{w}_b(t)^{\{n\times 1\}}, \boldsymbol{w}_r(t)^{\{n\times 1\}}\}$.

Appendix A.4. Temporal discretization

The temporal discretization requires the formulation of Equation (A.14) into the state space. The continuous-time state space model of Equation (A.14) can be written in the classical form:

$$\dot{\boldsymbol{x}}(t) = \boldsymbol{A}(t)\boldsymbol{x}(t) + \boldsymbol{B}\boldsymbol{u}(t) \tag{A.15}$$

where $\boldsymbol{x}(t)$, $\boldsymbol{A}(t)$ and $\boldsymbol{B}$ and $\boldsymbol{u}(t)$ are defined after [14] using the mass $\boldsymbol{M}^{\{2n\times 2n\}}$, damping $\boldsymbol{C}^{\{2n\times 2n\}}$ and stiffness $\boldsymbol{K}^{\{2n\times 2n\}}$ matrices, and the forcing term $\boldsymbol{f}(t)^{\{2n\times 1\}}$.
Equation (A.15) is then transformed in the following discrete form:

$$\dot{\boldsymbol{x}}_k = \boldsymbol{A}_k\boldsymbol{x}_k + \boldsymbol{B}\boldsymbol{u}_k \tag{A.16}$$

where k indicates the time step. Equation (A.16) is solved using the Dormand-Prince method based on an explicit Runge-Kutta temporal discretization [16].

Appendix B. Database of fatigue tests

Table B.8: Database of normal strength concrete fatigue tests taken from [50, 56, 25, 30, 23], where f_c is the concrete average strength in MPa, and C_{exp} is the experimental number of cycles to fatigue.

Ref	f_c	S_{cmin}	S_{cmax}	C_{exp}	Ref	f_c	S_{cmin}	S_{cmax}	C_{exp}	Ref	f_c	S_{cmin}	S_{cmax}	C_{exp}
	31.578	0.100	0.900	20		44.100	0.205	0.745	2086412		34.440	0.080	0.800	955
[50]	31.578	0.100	0.800	140		44.100	0.205	0.745	2399938		34.440	0.070	0.700	6026
	31.578	0.100	0.700	900		44.100	0.205	0.745	2613966		34.440	0.060	0.600	49545
	54.300	0.180	0.900	3		44.100	0.205	0.745	2722074		34.440	0.320	0.800	2432
	54.300	0.192	0.960	4		44.100	0.205	0.745	3431626		34.440	0.280	0.700	32137
	54.300	0.192	0.960	100		44.100	0.205	0.745	5030371		34.440	0.560	0.800	18365
	54.300	0.168	0.840	1050		44.100	0.205	0.745	6753051		34.440	0.080	0.800	298
	54.300	0.168	0.840	2000		44.100	0.205	0.745	6864359		34.440	0.070	0.700	1683
[56]	54.300	0.160	0.800	3000		44.100	0.205	0.745	6983932		34.440	0.060	0.600	11535
	54.300	0.160	0.800	6300		44.100	0.205	0.745	7099046		34.440	0.320	0.800	757
	54.300	0.140	0.700	8200		44.100	0.205	0.745	8641716		34.440	0.280	0.700	6166
	54.300	0.149	0.746	32000		44.100	0.205	0.745	8855233		34.440	0.560	0.800	2254
	54.300	0.149	0.746	40000		44.100	0.205	0.745	8949525		34.440	0.080	0.800	89
	54.300	0.139	0.693	650000		44.100	0.205	0.745	9038576		34.440	0.070	0.700	441
	41.000	0.095	0.633	1200000		44.100	0.205	0.745	14437766		34.440	0.060	0.600	2667
	41.000	0.100	0.667	1050000		44.100	0.205	0.745	15794286		34.440	0.320	0.800	140
	41.000	0.105	0.700	750000		44.100	0.205	0.745	25043787		34.440	0.280	0.700	1462
	41.000	0.113	0.750	320000		44.100	0.205	0.845	36		34.440	0.080	0.800	298
	41.000	0.271	0.713	4000000		44.100	0.205	0.845	40		34.440	0.070	0.700	1683
	41.000	0.285	0.750	1400000		44.100	0.205	0.845	46		34.440	0.060	0.600	11535
	41.000	0.285	0.750	1000000		44.100	0.205	0.845	69		34.440	0.320	0.800	757
	41.000	0.304	0.800	800000		44.100	0.205	0.845	79		34.440	0.280	0.700	6166
	41.000	0.323	0.850	220000		44.100	0.205	0.845	85		34.440	0.560	0.800	2254
	41.000	0.492	0.820	1400000		44.100	0.205	0.845	90		34.440	0.080	0.800	89
	41.000	0.520	0.867	600000		44.100	0.205	0.845	100		34.440	0.070	0.700	441
	41.000	0.540	0.900	46000		44.100	0.205	0.845	110		34.440	0.060	0.600	2667
[25]	41.000	0.540	0.900	320000		44.100	0.205	0.845	170		34.440	0.320	0.800	140
	41.000	0.668	0.867	2000000		44.100	0.205	0.845	250		34.440	0.280	0.700	1462
	41.000	0.672	0.873	4100000		44.100	0.205	0.845	290		36.408	0.070	0.700	5260
	41.000	0.683	0.887	2200000		44.100	0.205	0.845	310		36.408	0.060	0.600	44157
	41.000	0.693	0.900	1500000		44.100	0.205	0.845	410		36.408	0.320	0.800	4498
	41.000	0.708	0.920	3100000		44.100	0.205	0.845	500		36.408	0.280	0.700	76384
	41.000	0.708	0.920	230000	[30]	44.100	0.205	0.845	540		36.408	0.560	0.800	70795
	41.000	0.732	0.950	200000		44.100	0.205	0.845	640	[23]	36.408	0.060	0.600	6699
	41.000	0.774	0.880	2100000		44.100	0.205	0.845	960		24.026	0.070	0.700	6546
	41.000	0.792	0.900	2000000		44.100	0.205	0.845	980		24.026	0.060	0.600	95499
	41.000	0.792	0.900	3200000		44.100	0.205	0.845	1160		24.026	0.320	0.800	5395
	41.000	0.810	0.920	160000		44.100	0.205	0.845	1420		24.026	0.280	0.700	539511
	41.000	0.836	0.950	70000		44.100	0.205	0.845	1440		24.026	0.560	0.800	67453
	44.100	0.205	0.745	643132		44.100	0.205	0.845	1600		24.026	0.060	0.600	7345
	44.100	0.205	0.845	1065		44.100	0.205	0.845	2071		30.996	0.070	0.700	85704
	44.100	0.050	0.805	483		44.100	0.205	0.845	3269		30.996	0.080	0.800	6501
	44.100	0.050	0.685	51464		44.100	0.205	0.845	3851		30.996	0.090	0.900	1067
	44.100	0.050	0.585	2746629		44.100	0.205	0.845	4181		30.996	0.360	0.900	4898
	44.100	0.200	0.880	93		44.100	0.205	0.845	5332		30.996	0.630	0.900	81283
	44.100	0.200	0.840	1293		44.100	0.205	0.845	8813		30.996	0.080	0.800	925
	44.100	0.200	0.780	66573		44.100	0.205	0.845	9283		33.784	0.070	0.700	7112
	44.100	0.200	0.740	921298		44.100	0.205	0.845	30896		33.784	0.060	0.600	58749
	44.100	0.200	0.680	47435120		44.100	0.205	0.845	34522		33.784	0.320	0.800	3793
	44.100	0.350	0.890	1257		44.100	0.205	0.845	46784		33.784	0.280	0.700	80353
	44.100	0.350	0.850	120420		44.100	0.205	0.845	296961		33.784	0.560	0.800	95940
	44.100	0.400	0.910	105		44.100	0.205	0.845	438430		33.784	0.060	0.600	3565
	44.100	0.400	0.875	52650		44.100	0.050	0.805	483		44.362	0.070	0.700	4140
	44.100	0.400	0.835	63841047		44.100	0.050	0.685	51464		44.362	0.060	0.600	48084
	44.100	0.205	0.745	330		44.100	0.050	0.585	2746629		44.362	0.320	0.800	3828
	44.100	0.205	0.745	1960		44.100	0.200	0.880	93		44.362	0.280	0.700	78163
	44.100	0.205	0.745	11439		44.100	0.200	0.840	1293		44.362	0.560	0.800	85310
[30]	44.100	0.205	0.745	11874		44.100	0.200	0.780	66573		44.362	0.060	0.600	3428
	44.100	0.205	0.745	12874		44.100	0.200	0.740	921298		35.000	0.070	0.700	8147
	44.100	0.205	0.745	23747		44.100	0.200	0.680	47435120		35.000	0.060	0.600	44259
	44.100	0.205	0.745	39902		44.100	0.350	0.890	1257		35.000	0.280	0.700	67764
	44.100	0.205	0.745	44463		44.100	0.350	0.850	120420		35.000	0.070	0.700	1524
	44.100	0.205	0.745	70226		44.100	0.400	0.910	105		35.000	0.060	0.600	21878
	44.100	0.205	0.745	79891		44.100	0.400	0.875	52650		35.000	0.280	0.700	6209
	44.100	0.205	0.745	115213		44.100	0.400	0.835	63841047		35.000	0.070	0.700	5358
	44.100	0.205	0.745	117166		36.900	0.000	0.900	129		35.000	0.060	0.600	527
	44.100	0.205	0.745	146791		36.900	0.000	0.800	465		35.000	0.280	0.700	4385
	44.100	0.205	0.745	287607		36.900	0.000	0.700	1959					
	44.100	0.205	0.745	534687		36.900	0.000	0.600	16904					
	44.100	0.205	0.745	924911		36.900	0.000	0.500	167109					
	44.100	0.205	0.745	1025416	[23]	36.900	0.360	0.900	245					
	44.100	0.205	0.745	1178148		36.900	0.320	0.800	2032					
	44.100	0.205	0.745	1474009		36.900	0.280	0.700	31696					
	44.100	0.205	0.745	1562788		36.900	0.720	0.900	465					
	44.100	0.205	0.745	1630797		36.900	0.640	0.800	25293					
	44.100	0.205	0.745	1953890		36.900	0.600	0.750	981748					

Appendix C. Posterior statistics of Θ

Table C.9: Posterior statistics of $\boldsymbol{\Theta}$ for the proposed model.

teta	Estimate	SE	Correlation coefficient																													
			θ_{000}	θ_{100}	t200	θ_{300}	θ_{010}	t210	θ_{310}	θ_{020}	t320	θ_{030}	θ_{130}	t230	θ_{330}	θ_{001}	θ_{101}	θ_{201}	θ_{301}	θ_{011}	θ_{211}	θ_{311}	θ_{021}	θ_{331}	θ_{002}	θ_{302}	θ_{012}	θ_{332}	θ_{003}	θ_{203}	θ_{303}	θ_{013}
θ_{000}	573.79	280.10	1.00																													
θ_{100}	-33.38	15.43	-0.47	1.00																												
θ_{200}	0.79	0.52	0.05	-0.81	1.00																											
θ_{300}	-0.01	0.01	0.00	0.48	-0.85	1.00																										
θ_{010}	-823.74	943.88	-0.65	-0.30	0.44	-0.13	1.00																									
θ_{210}	0.21	0.54	0.54	0.02	-0.58	0.79	-0.36	1.00																								
θ_{310}	0.02	0.02	0.01	0.13	0.20	-0.68	-0.33	-0.64	1.00																							
θ_{020}	1281.91	1307.94	0.52	0.34	-0.34	-0.07	-0.96	0.11	0.55	1.00																						
θ_{320}	-0.03	0.02	-0.35	-0.19	0.16	0.29	0.64	0.10	-0.83	-0.76	1.00																					
θ_{030}	-895.20	711.98	-0.59	0.25	-0.20	0.44	0.51	0.14	-0.64	-0.58	0.71	1.00																				
θ_{130}	20.02	43.15	0.27	-0.73	0.58	-0.35	0.37	-0.11	-0.02	-0.38	0.11	-0.49	1.00																			
θ_{230}	-0.67	1.06	-0.38	0.76	-0.50	0.19	-0.29	-0.12	0.24	0.37	-0.22	0.40	-0.95	1.00																		
θ_{330}	0.02	0.01	0.65	-0.42	0.16	-0.25	-0.37	0.20	0.35	0.37	-0.61	-0.82	0.57	-0.59	1.00																	
θ_{001}	-949.23	1418.15	0.02	0.15	-0.12	-0.01	-0.18	0.01	0.19	0.21	-0.26	-0.50	0.37	-0.40	0.56	1.00																
θ_{101}	247.17	107.19	0.25	-0.30	0.23	-0.12	-0.10	0.14	-0.12	0.06	0.05	0.34	-0.41	0.33	-0.22	-0.78	1.00															
θ_{201}	-6.97	3.86	-0.12	0.44	-0.51	0.32	-0.09	0.04	0.21	0.11	-0.30	-0.37	0.21	-0.08	0.22	0.52	-0.84	1.00														
θ_{301}	0.05	0.05	-0.03	-0.44	0.59	-0.36	0.24	-0.16	-0.30	-0.25	0.51	0.41	-0.06	-0.07	-0.29	-0.35	0.61	-0.93	1.00													
θ_{011}	-5448.08	2472.46	-0.47	-0.06	0.25	-0.05	0.62	-0.38	-0.28	-0.63	0.67	0.44	0.14	-0.04	-0.66	-0.40	-0.13	0.02	0.18	1.00												
θ_{211}	0.95	2.83	-0.14	-0.37	0.60	-0.41	0.27	-0.26	-0.21	-0.26	0.47	0.25	0.13	-0.26	-0.12	0.06	0.23	-0.71	0.89	0.13	1.00											
θ_{311}	0.02	0.06	0.22	0.33	-0.57	0.34	-0.36	0.29	0.32	0.36	-0.64	-0.36	-0.12	0.23	0.32	0.05	-0.19	0.67	-0.89	-0.37	-0.96	1.00										
θ_{021}	3480.24	2163.98	0.44	0.19	-0.45	0.21	-0.61	0.43	0.33	0.62	-0.76	-0.49	-0.15	0.11	0.64	0.34	-0.01	0.30	-0.54	-0.91	-0.53	0.72	1.00									
θ_{331}	-0.02	0.01	-0.30	-0.10	0.28	-0.03	0.40	-0.22	-0.45	-0.46	0.80	0.51	0.00	-0.03	-0.70	-0.32	0.06	-0.33	0.56	0.79	0.51	-0.72	-0.91	1.00								
θ_{002}	-507.91	784.83	0.13	0.05	-0.10	-0.01	-0.23	0.15	0.17	0.26	-0.37	-0.28	0.05	-0.12	0.50	0.45	-0.18	0.12	-0.14	-0.59	0.03	0.15	0.54	-0.57	1.00							
θ_{302}	0.01	0.01	0.10	-0.20	0.17	-0.04	0.07	0.01	-0.18	-0.13	0.27	0.10	0.07	-0.07	-0.22	-0.18	0.17	-0.20	0.22	0.26	0.09	-0.20	-0.29	0.41	-0.79	1.00						
θ_{012}	-281.14	993.96	-0.24	0.08	0.02	0.08	0.25	-0.17	-0.21	-0.28	0.45	0.41	-0.17	0.24	-0.68	-0.51	0.14	-0.08	0.14	0.70	-0.04	-0.18	-0.64	0.71	-0.90	0.53	1.00					
θ_{332}	0.01	0.01	0.12	-0.08	0.02	-0.15	-0.10	0.02	0.34	0.18	-0.52	-0.41	0.21	-0.20	0.65	0.35	-0.14	0.18	-0.27	-0.53	-0.12	0.33	0.57	-0.80	0.71	-0.57	-0.85	1.00				
θ_{003}	1636.35	789.06	0.09	-0.15	0.16	-0.21	-0.04	-0.07	0.21	0.10	-0.27	-0.23	0.15	-0.18	0.43	0.13	0.11	-0.14	0.07	-0.38	0.19	-0.02	0.27	-0.45	0.19	-0.18	-0.40	0.62	1.00			
θ_{203}	-1.09	1.11	0.12	-0.02	-0.11	0.12	-0.02	0.14	0.00	-0.02	-0.09	-0.11	0.09	-0.02	0.03	0.00	-0.16	0.30	-0.34	0.12	-0.44	0.38	0.10	-0.10	-0.18	0.36	0.04	-0.02	-0.55	1.00		
θ_{303}	0.01	0.02	-0.16	0.09	0.05	-0.06	0.02	-0.12	-0.02	0.02	0.11	0.15	-0.14	0.07	-0.09	-0.02	0.13	-0.25	0.29	-0.08	0.39	-0.34	-0.11	0.13	0.24	-0.48	-0.01	-0.03	0.41	-0.98	1.00	
θ_{013}	-421.32	526.93	-0.10	0.04	0.03	0.07	0.07	-0.01	-0.29	-0.13	0.45	0.32	-0.15	0.11	-0.49	-0.13	0.06	-0.18	0.31	0.35	0.23	-0.39	-0.44	0.70	-0.33	0.40	0.51	-0.86	-0.75	0.04	0.03	1.00